THE ROLE OF MECHANICAL STRATIGRAPHY IN FRACTURE INTENSITY AND DISTRIBUTION IN THE MISSISSIPPIAN TURNER VALLEY FORMATION; AN EXPERIMENTAL EVALUATION

By

MORGAN WITTSTOCK

B.Sc with Honours, University of British Columbia, 2010

A THESIS SUBMITTED IN PARTIAL FULFILLMENT OF
THE REQUIREMENTS FOR THE DEGREE OF

BACHELOR OF SCIENCE (HONOURS)

in

THE FACULTY OF SCIENCE

(Earth and Ocean Sciences)

This thesis conforms to the required standard

……
Supervisor

THE UNIVERSITY OF BRITISH COLUMBIA

(Vancouver)

MARCH 2009

ABSTRACT

The purpose of this thesis is to study the relationship between composition and texture on rock strength and fracture geometry in the Mississippian Turner Valley Formation. Samples from the three major units of the Mississippian Turner Valley Formation, the Mt1, Mt2 and Mt3, were deformed using the large sample deformation rig and mechanical strength was determined. Experimental data as well as microscopic and macroscopic observations were compared to natural fracture data from the Jumping Pound West Reservoir. Results were also compared to permeability data from core samples in order to contrast deformation style with fracture connectivity. Dolomitic samples from the Mt1 and Mt3 were found to be the strongest as well as fracture the most favourably with respect to fluid flow. Stronger samples were also found to correlate with high permeability within the core. Applying the study results will enable us to improve existing fracture models within the Jumping Pound West Reservoir and better predict regions of fluid flow within fractured reservoirs. Understanding mechanical strength in the reservoir will also provide insight into placing hydrofractures in order to maximize well performance in oil and gas reservoirs.

TABLE OF CONTENTS

LIST OF FIGURES

LIST OF TABLES

LIST OF APPENDICES

The Role of Mechanical Stratigraphy in Fracture Intensity and Distribution in the Mississippian Turner Valley Formation; an Experimental Evaluation

By: Morgan Wittstock

March 30, 2009

1. BACKGROUND AND INTRODUCTION

The purpose of this thesis is to study the relationship between composition and texture on rock strength and fracture geometry in the Mississippian Turner Valley Formation in order to further understand fracture formation in natural fold and thrust belts. Samples from the three major units of the Mississippian Turner Valley Formation, the Mt1, Mt2, and Mt3, will be deformed using a triaxial rock press. The resulting mechanical data for each unit will be compared with known permeabilities to test the hypothesis that strong rocks will contain more fractures than relatively weak rocks. Experimental data will also be compared to observations of natural fractures (Wittstock, unpublished manuscript, 2008) within the Jumping Pound West Reservoir with the aim of improving existing models for fracture connectivity. Fracture connectivity is important for reservoir quality in tight reservoirs where connected porosity is limited. Due to variability in carbonate reservoirs not all structurally similar exploration targets are highly fractured (Miller et. al., 2007).

The Mississippian Turner Valley Formation (Mtv) is a cold water carbonate facies unit found in the south west of the Western Canadian Sedimentary Basin (WCSB). The WCSB extends from eastern British Columbia into Manitoba. In Alberta it blankets the entire province. The Mtv outcrops at Moose Mountain, fifty kilometers southwest of Calgary and is present in the subsurface in the Jumping Pound West Area southwest of Cochrane, Alberta (Figure 1). Mississippian Turner Valley Formation rocks are distributed throughout the foothills belt of Western Alberta. The Formation thins to the east of Calgary. To the west, in the Rocky Mountain front ranges, the stratigraphic equivalent is the Livingstone Formation which also encompasses the Pekisko and Shunda formations (Glass, 1997). Figure 1 shows the approximate subsurface extent of the Turner Valley Formation. Jumping Pound West is a carbonate gas reservoir originally discovered in 1961. The reservoir is mature and has

produced 57 bcm out of an estimated 64 bcm total. Pressure in the field has dropped from an initial 30 Mega Pascals (MPa) to about 6 MPa. Average porosity ranges from three to six percent. As the reservoir is depleted and flowing wells become harder to find, fracture permeability is becoming increasingly important in well success (Wittstock, unpublished manuscript, 2008).

Structurally, the Jumping Pound West and Moose Mountain areas are imbricated thrust sheets formed during the Laramide Orogeny in the Late Cretaceous and Early Tertiary. The Jumping Pound West area exhibits a fault bend fold structural style with fracture concentrations in crestal and paleocrestal areas on these structures. At a reservoir scale, these fractures lead to regions of increased permeability and inflow into wells (Wittstock, unpublished manuscript, 2008). Due to textural and mineralogical heterogeneity within the Mississippian Turner Valley Formation (Mtv), the role of small scale heterogeneities with respect to fracturing and permeability creation is not fully understood.

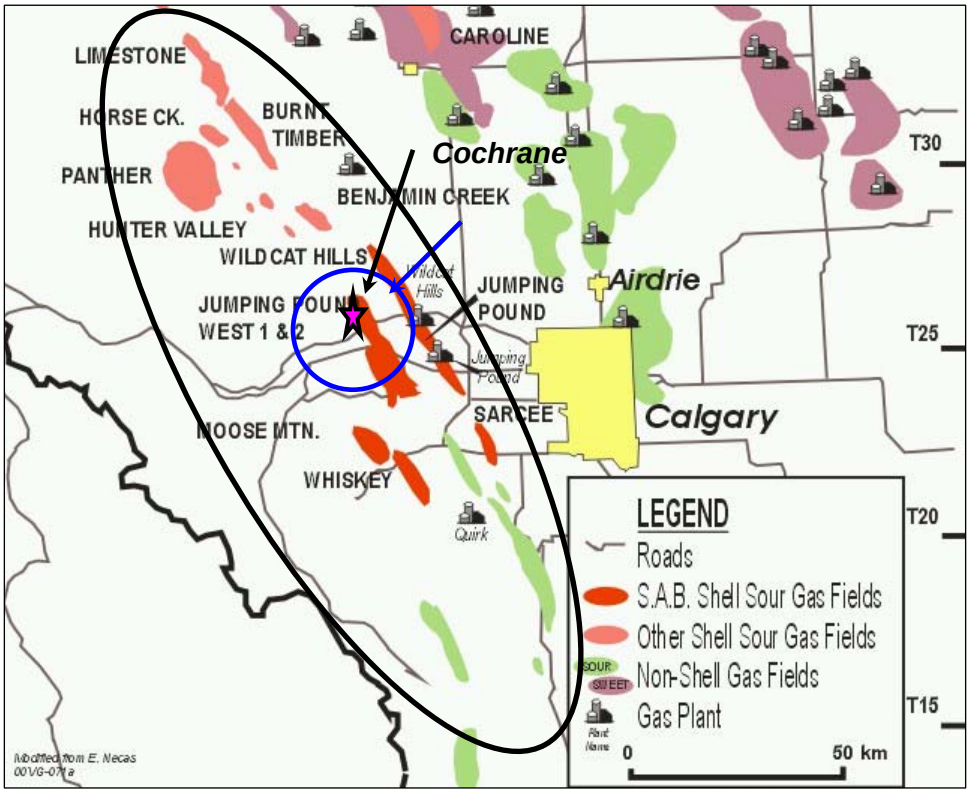

Figure 1: Map of Western Alberta Gas Fields. Jumping Pound West is highlighted in blue and study well 0/2-19-26-6 is highlighted by a star. Approximate regional extend of the Mississippian Turner Valley is highlighted by a black oval. Modified from an unpublished figure by Anonymous (2008).

1.1 Stratigraphy

Mississippian Turner Valley stratigraphy is significant in this study because lithology and textural features are very important in testing a mechanical stratigraphy model. The mechanical stratigraphy of a rock unit is strongly dependent on thickness, lithology and the nature of the contacts between adjacent rock units (Cooke and Underwood, 2001). Most units in the carbonate complex of the Western Canadian Sedimentary Basin, such as the Mtv, are large scale carbonate sheets and are internally complex because of facies changes and high frequency allo and autocyclic processes that occurred during deposition (Martindale and Boreen, 1995). Mississippian Turner Valley formation rocks are interpreted to be part of a shelf complex in a cool water carbonate succession (Martindale and Boreen, 1995). Figure 2 illustrates the facies relationships between the Mississippian Turner Valley units and highlights the depositional variability in the Formation. The Mtv is placed in the upper and middle shelf region. Variability in depositional environments and a series of third order sea level changes has introduced significant complexity into the rock record and into the mechanical stratigraphy of the units. Core logging completed on behalf of Shell Canada has shown meter scale cyclicity in deposition and lithology. Figure 3 illustrates the general subdivision of the Mississippian Turner Valley into the Mt1, Mt2, and Mt3. The Mt3 member is further divided into Mt3a, b, and c. The overall lithology of the Mt1 and Mt3 members in the Turner Valley is a medium to coarse grained crystalline crinoidal limestone and medium grained crystalline dolomite and are identified by their relatively clean gamma ray readings (Eggenkamp, unpublished manuscript, 2006). The Mt2, a finely crystalline non-porous argillaceous carbonate (Glass, 1997), separates these units. It is easily identifiable from gamma logs by two distinct spikes (Figure 3) and is the most recessive in the Turner Valley (Glass, 1997).

Textural heterogeneities within units are large influences on mechanical stratigraphy and fracture control (Di Naccio et. al., 2005). As there is significant heterogeneity in the Mississippian Turner Valley, we expect a large variation in mechanical strength throughout the reservoir. Fractures will tend to initiate on flaws such as vuggy porosity (Cooke et. al., 2006). Crinoid fossils in the Mt1 and Mt3 are sources of vuggy porosity. Dissolution of

fossils occurred during diagenesis and many voids were left unfilled by subsequent processes. Mt3 exhibits significant amounts of vuggy porosity, which allows for the initiation of fractures (Cooke et. al., 2006). Porosity in the Mt1 is slightly lower than in the Mt3 in the study well. Fossomoldic porosity is common in the formation in general (Glass, 1997) and a reduction of overall porosity is likely consistent with an overall reduction in fossomoldic porosity. Overall, dolomitization will increase mechanical strength and lead to a larger degree of brittle failure (Austin et. al., 2005). Dolomitization is patchy within the Mtv but overall the Mt3a is the most fractured and consistently dolomitized in the Jumping Pound West Field. Detachment of thrusting in the area is along the underlying shaly Exshaw Formation and the Nordegg above (Fermor, 1999). The Nordegg is therefore expected to act as a strain dissipater with respect to the Mtv and be mechanically weak (Figure 4). The Shunda Formation is also likely to be mechanically weaker than the Mississippian Turner Valley because of its mudstone lithology. Hence, the Mtv will act as the mechanically strong unit and accommodate the majority of the brittle deformation.

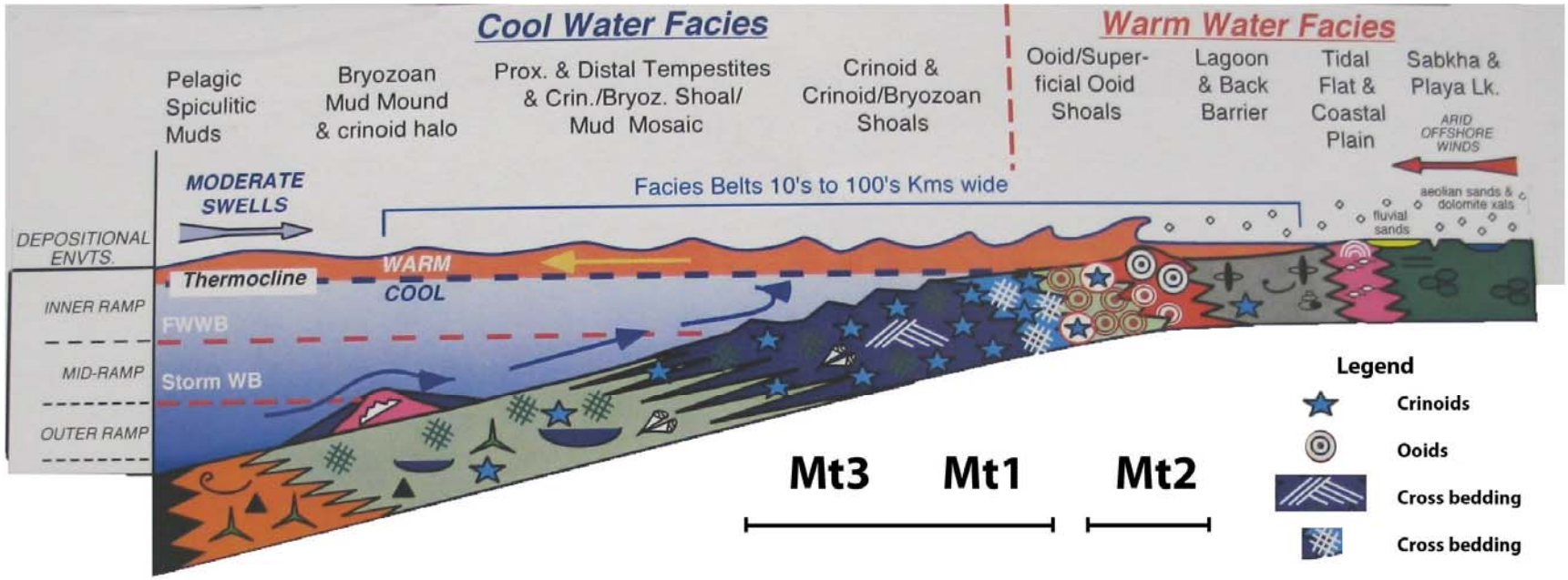

Figure 2: Depositional environment of the Mississippian Turner Valley highlighting facies variability within the Formation. Crinoid rich depositional environments were preserved with significant fossomoldic porosity. All units were variably dolomitized during diagenesis. Modified from Martindale and Boreen (2005).

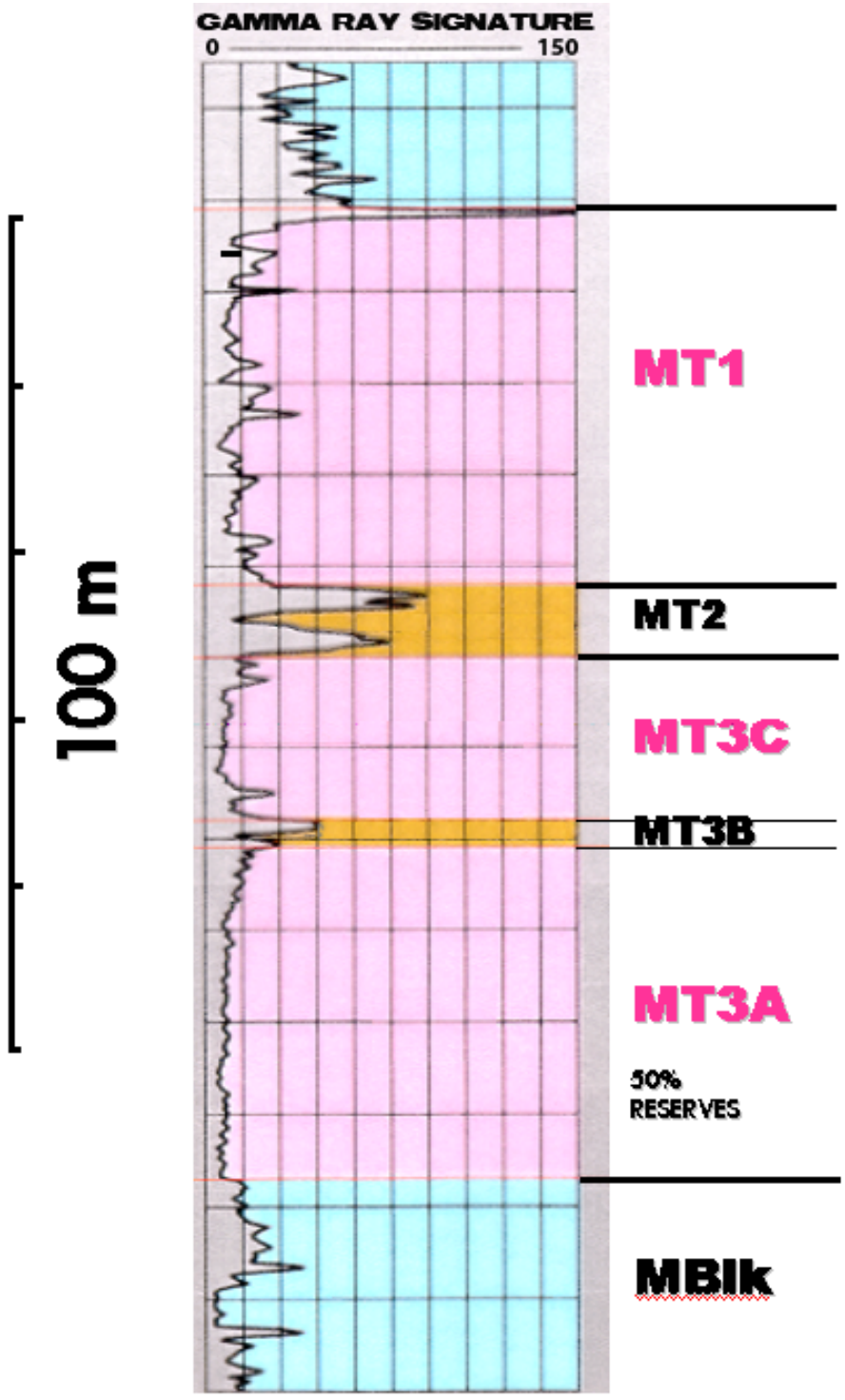

Figure 3: Gamma ray log from the Mtv showing individual members. Mt2 is highlighted by a significant gamma ray spike (orange) indicating a strong argillaceous component. Modified from an unpublished figure by J. Ruelle (2008).

Era	Period	Group	Formation	Members	Lithology
Mesozoic	Jurassic		Kootenay		
		Fernie	Passage Beds		
			Fernie Shale		Shale
			Nordegg		Limestone, Shale
Paleozoic	Mississippian	Rundle	Turner Valley	Mt1	**Upper porous dolomite**
				Mt2	Middle dense shale
				Mt3c	**Lower porous/Elkton dolomite**
				Mt3b	
				Mt3a	
			Shunda		Argillaceous anhydritic dolomitic limestone
			Pekisko		Limestone
			Banff		
			Exshaw		Black Shale
	Devonian	Wabamun	Big Valley		
			Stettler	Upper Porous	Dolomite and anhydrite
				Upper Tight	
				Crossfield	Dolomite and anhydrite
				Lower	
		Fairholme	Calmar		Biostromal and biohermal calcites and dolomites with argillaceous sections
			Nisku		
			Ireton		
			Leduc		

Figure 4: Stratigraphic column of the rocks of the Jumping Pound area west of Calgary showing the Mississippian Turner Valley with respect to the rest of the stratigraphic column. Studied units are highlighted in red. Modified from an unpublished figure by Anonymous (2008)

1.2 Thin Skinned Fold and Fault Related Regional Structure of the Sample Locality

Samples used in this study are from the Jumping Pound West field located in the Canadian Foothills fold and thrust belt of the Western Canadian Sedimentary Basin (Figure 1). The Foothills west of Calgary are associated with the easternmost belts of deformation caused by the Laramide Orogeny (Eggenkamp, unpublished manuscript, 2007). Jumping Pound West consists of five westward dipping imbricate thrust sheets that carry Mississippian age rocks. Mississippian units are underthrusted beneath previously intensely deformed Jurassic and Cretaceous rocks (Wittstock, unpublished manuscript, 2008). Regional structural trend is consistent with overall Canadian Rockies structure and fold axes trend NNE-SSW (Fermor, 1999). Closely spaced, steeply dipping thrust sheets of Jurassic and Cretaceous rocks comprise the surface expression in the Jumping Pound area. Detachment of the Mesozoic rocks occurs within the shales of the Fernie Group (Figure 4) and does not involve the stratigraphically lower Paleozoic Rocks. Under-thrusted Paleozoic carbonates, including the Mtv, consist of shallowly dipping imbricated thrust sheets (Figure 5). Detachment is inferred to have occurred along the Mississippian Exshaw Formation and does not involve the underlying Precambrian crystalline basement (Fermor, 1999) or Devonian age rocks. Compression was accommodated by fault bend folding (Figure 6). Deformation terminates just to the east in the Triangle zone which consists of Mesozoic fault slices wedged into the Western margin of the Western Canadian Sedimentary Basin (Fermor, 1999).

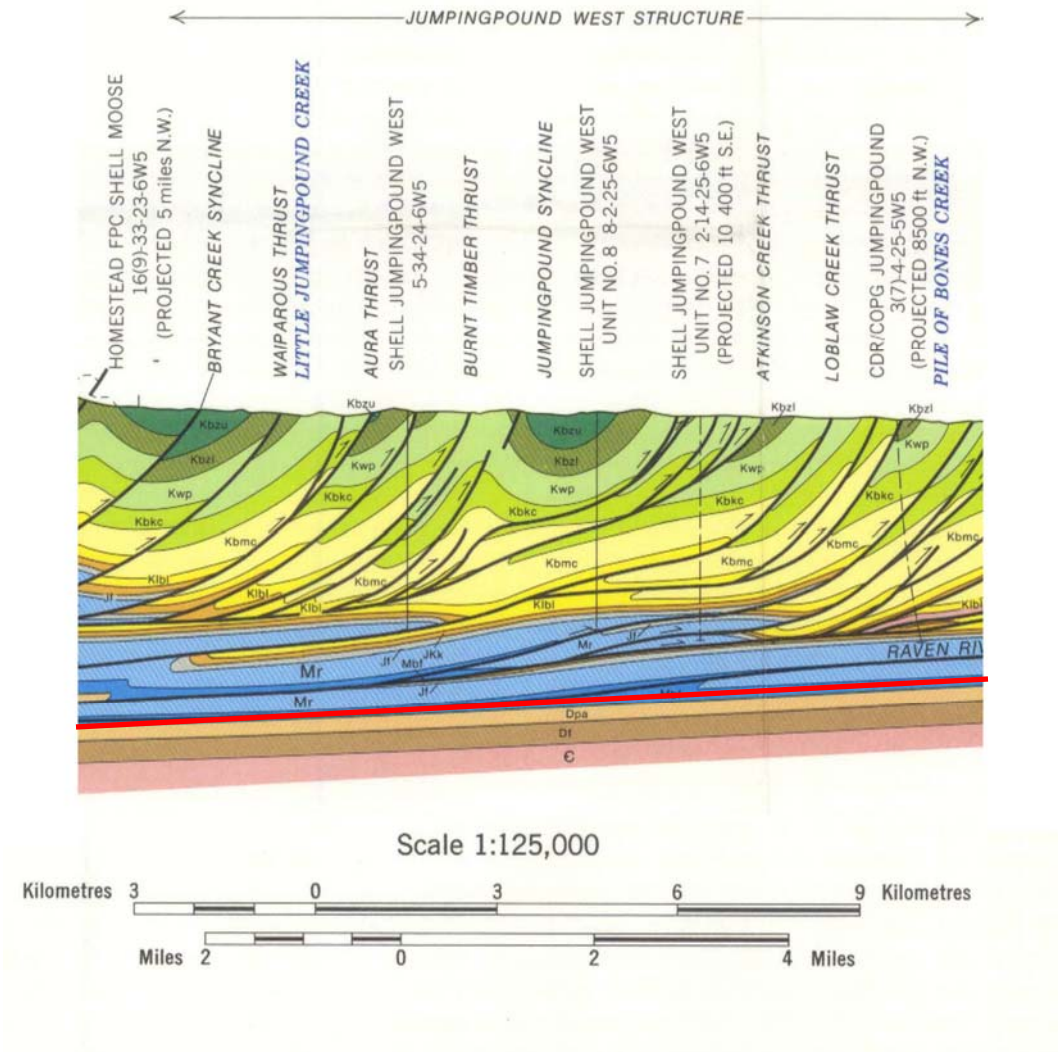

Figure 5: Cross-Section of the Jumping Pound West Area. Modified from Ollerrenshaw (1978). Lower detachment surface is highlighted in red.

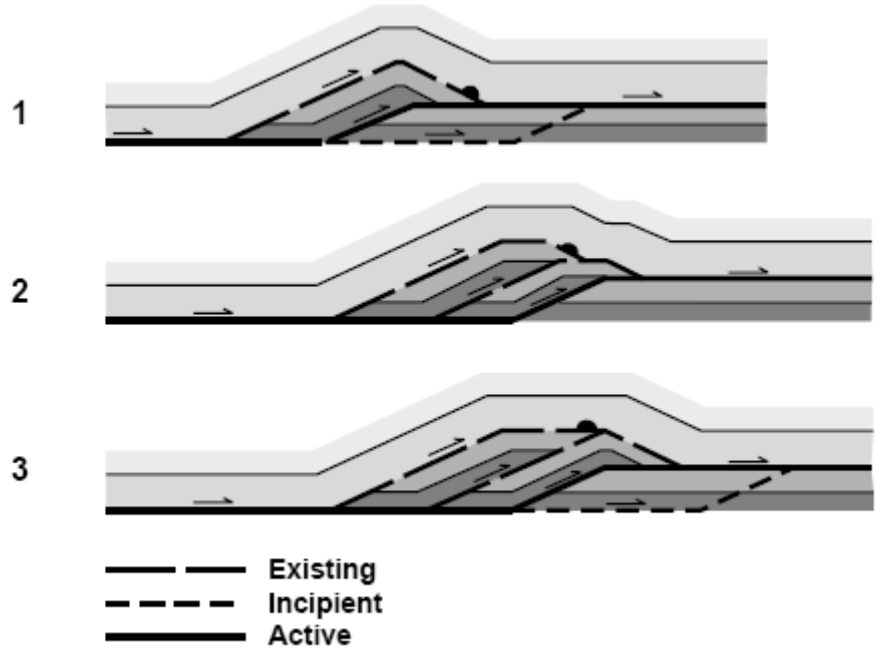

Figure 6: Imbricate Fault Bend Fold Model (Fermor, 1999). The black dot tracks the original fold front of the first fold as it is back-rotated by further thrusting.

1.3 Natural Fracture Constraints in the Jumping Pound West Reservoir

Fracture intensity was constrained on a reservoir scale in order to create a representative fracture model of Jumping Pound West (Wittstock, unpublished manuscript, 2008). The Jumping Pound West natural gas reservoir is a low permeability reservoir with permeabilities in the range of 0.1 to 1 millidarcies (mD). Permeability for the reservoir was determined by core testing conducted by Shell Canada. Due to this low permeability, fracture connectivity is very important in the successful exploitation of subsurface resources. Two main fracture orientations of interest exist in the Jumping Pound West reservoir. The first is an axial parallel set that runs parallel to the north northwest-south southeast regional structural trend. The second and most abundant set trends in a 45^{o} range around a modal azimuth of 045 and is referred to as the cross axial set. A third set is present in some of the wells in the area and is consistent with local fault orientations (Figure 7). All sets dip steeply at a mean dip of 70^{o}. All discussed fractures

are inferred to be Mode I extensional fractures. Some fractures in the wellbore are more shallowly dipping than the axial parallel and cross axial sets and are inferred to be shear fractures. Flow is not expected along these fractures so they were not the focus of the study (Wittstock, unpublished manuscript, 2008). Axial parallel fractures, the set inferred to flow gas, are concentrated in paleocrestal areas of folds due to a reversal of stress orientations along the crest. Extensional fractures form in the hinge area associated with folding (Figure 8) (Stephenson et. al., 2007). The abundant 045 trending set is pervasive but concentrated in the forelimb of structures (Wittstock, unpublished manuscript, 2008).

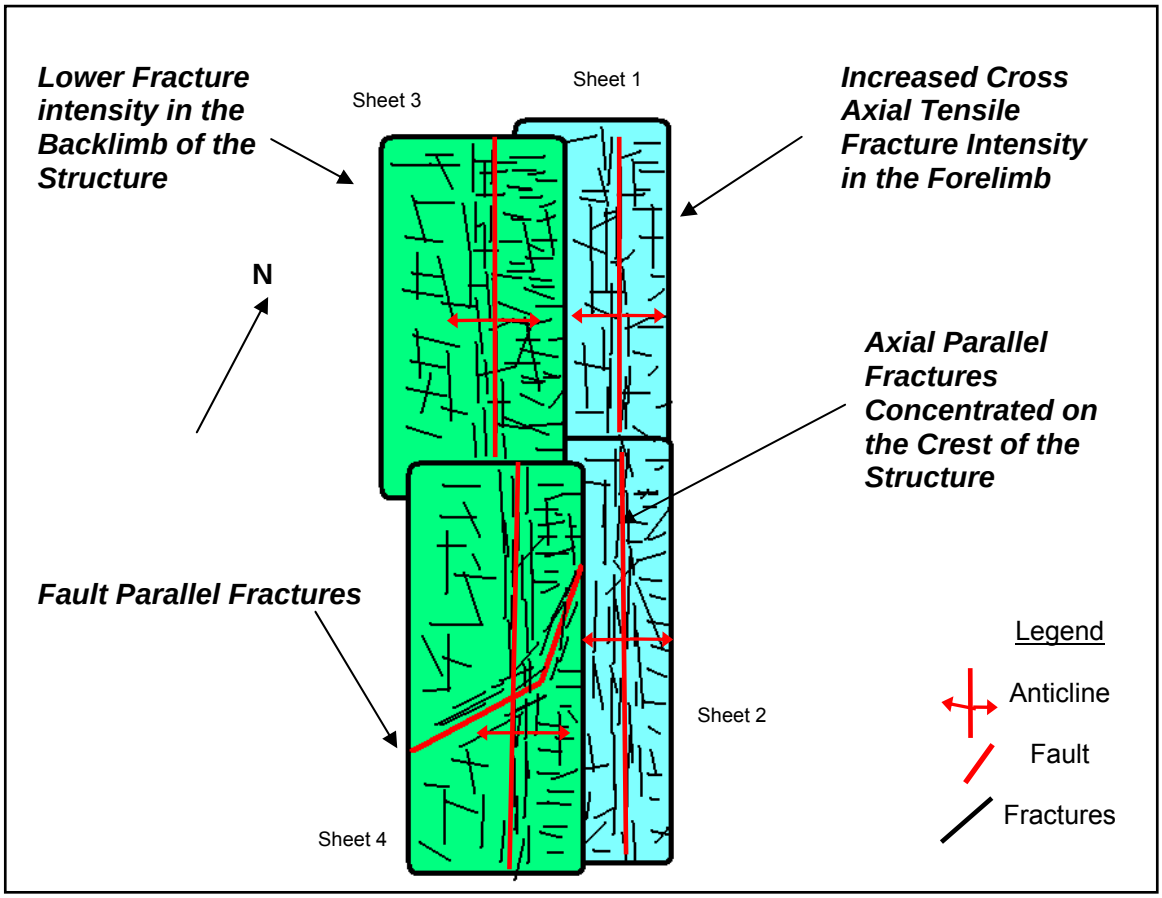

Figure 7: Schematic of fracturing in the Jumping Pound West Field.

As a result of the imbrication and therefore back-rotation in the Alberta foothills, many paleo-crestal areas are no longer at topographic highs. It is possible to determine the location of paleo-crests based on the relationship between flats and ramps in

structural cross section (Figure 6)**.** On a large scale, the structures allow the prediction of fracture connectivity and allow a relative model to be created. Small scale heterogeneities in the rocks complicate this model. Overall the crystalline Mt3 is generally the most fractured and Mt2 is the least. This is consistent with mineralogy and lithology. Argillaceous material is minimal in the Mt3 while in the Mt2, the argillaceous input is consistently higher because of a different depositional environment (Figure 2). Mt3 represents a mechanically stronger unit on a reservoir scale and will accommodate deformation by brittle processes and fracture. However, there is a large degree of variability within each unit. Determining the mechanical strength of the rocks should better constrain the model at smaller scales.

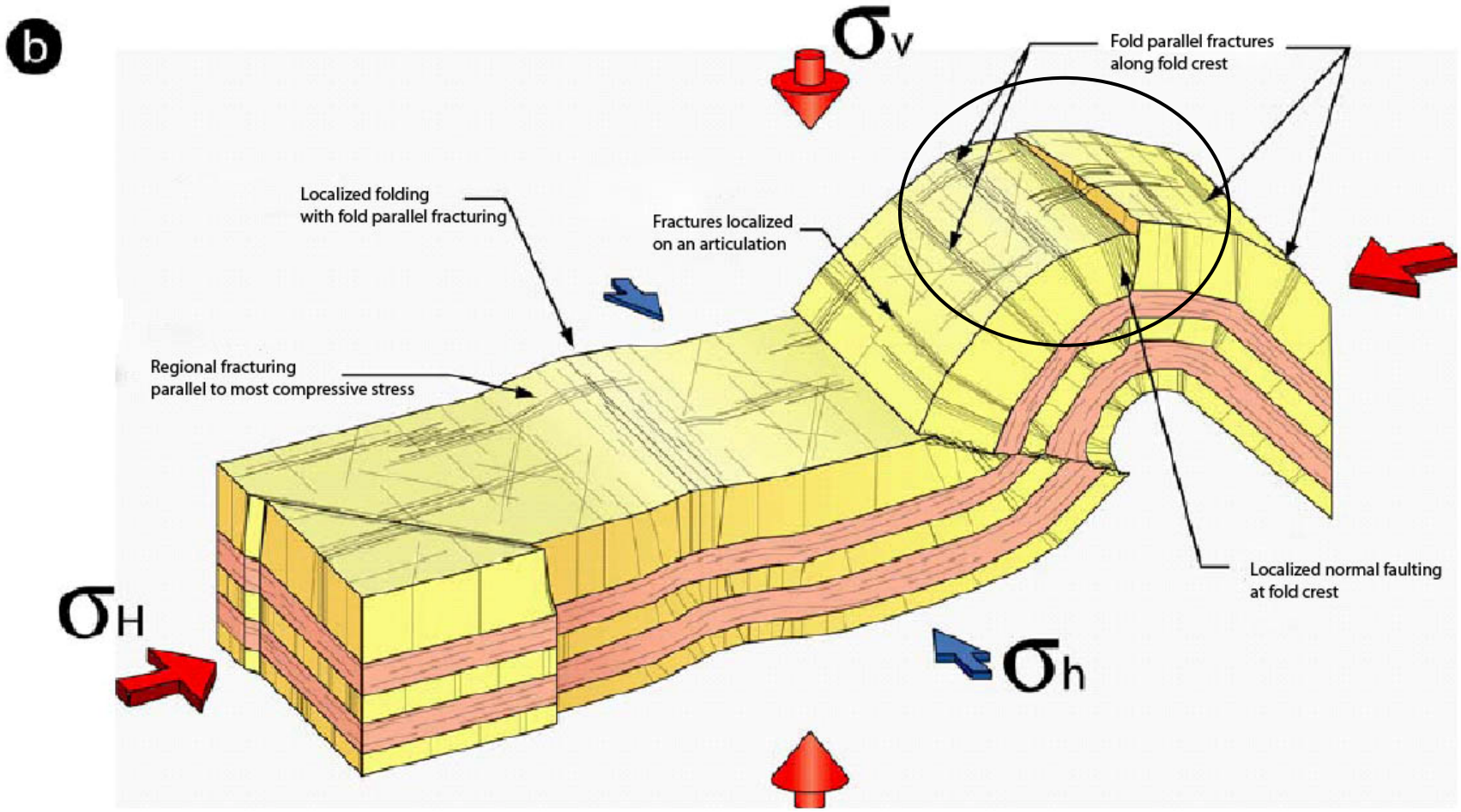

Figure 8: Expected fracture orientations in a compressional fold regime. Circled area highlights the crestal area which includes fold parallel fractures, modified from Bazalgette (2004).

1.4 Previous Work on the Mechanical Strength of Carbonates

Dolomite is exceptionally strong and will not undergo twinning or other crystal plastic processes at room temperate regardless of confining pressure (Austin et. al., 2005). Austin et. al. (2005) considered porosity and grain size to be major textural effects on rock strength. At low temperatures and constant confining pressures, grain size is inversely related to peak stress (Fredrich et. al., 1990). Grain boundary textures were also found to be major influences on the nature of deformation. The type of boundary relationship between grains can inhibit or promote the ability of grains to shear with respect to one another while intragranular flaws such as cleavage will encourage intragranular deformation. Increasing the degree of interlocking along grain boundaries will decrease the ability of grains to rotate past one another. Austin et. al. (2005) also found that in dolomite with porosities less that 7%, pore collapse is not a major factor in deformation type and the conversion from brittle to cataclastic flow.

In contrast to dolomite, calcite can deform by mechanical twinning at 296K and the development of intragranular deformation is very common in limestones. The mechanism of deformation in calcite is strongly dependent on texture and porosity. Shear compaction and pore collapse are observed in limestones with porosity as low as 3% prior to fracturing (Baud et. al., 2000). Brittle fracture and the generation of a macroscopic shear plane occurs as a multi stage process; a) the development of Mode I cracks, b) the formation of wing tip cracks at the tips of Mode I fractures due to shear stress and c) the coalescence of these cracks into a shear fracture (Baud et. al., 2000).

2. EXPERIMENTAL ROCK DEFORMATION

2.1 Methodology

2.1.1 Starting Material

Core samples studied are from well number 0/2-19-26-6 located in the north end of the Jumping Pound West field (Figure 1). Samples from the three major subdivisions of the Mississippian Turner Valley, the Mt1, Mt2 and Mt3, were collected in order to perform deformation experiments. Samples were chosen for their hand sample scale textural consistency when possible. In order to characterize the samples, bulk chemical composition was analysed using x-ray fluorescence for each Mtv member and texture and mineralogy of the initial rock was observed in thin section. Porosity for each sample was also measured using the helium pycnometer in the VPL at UBC.

2.1.1a X-ray Fluorescence

Whole rock analysis was performed at ALS Chemex in North Vancouver, British Columbia using X-ray fluorescence. Rocks were analysed for major rock forming oxides including MgO CaO, SiO_2, and Al_2O_3. Analysis is based on the assumption that, in non-mineralized rocks, major rock forming oxides should make up close to 100% of the rock. Loss on ignition is also recorded (ALS Chemex, 2009). XRF analysis is tabulated in Appendix A.

2.1.1b Helium Pycnometry

Connected porosity was measured using the Helium Pycnometer in the Volcanology and Petrology laboratory at the University of British Columbia. In order to calculate porosity, the bulk sample volume is obtained by measuring the diameter and length of the core and calculating volume. The measured sample volume is then obtained

by determining the amount of space that the sample takes up in a pycnometer cell of known volume with respect to a reference cell. To increase accuracy, helium is used instead of air because it is a smaller molecule. A detailed procedure is outlined by K. Michol (2008). Porosity is then calculated based on the following relationship between bulk volume and measured volume:

$$\Phi=1-V_{sample}/V_{bulk}*100$$

Measurements taken by the pycnometer are considered to be accurate to within 05-1.0% (Russell, Personal Communication, 2009). Figure 9 shows the pycnometer setup.

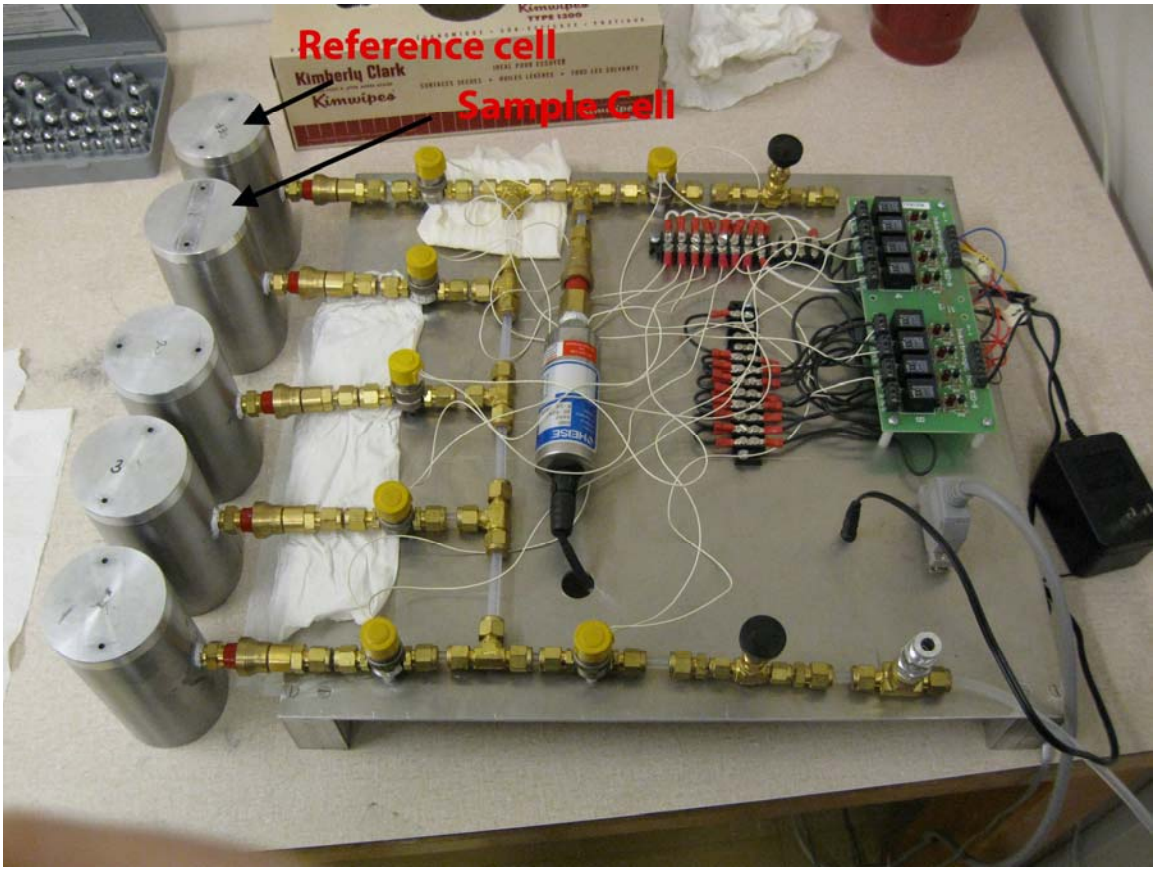

Figure 9: Helium Pycnometer in the VPL

2.1.1c Mineralogy and Texture

Mineralogy and rock texture were assessed in thin section and hand sample for each deformed sample. Mineralogy was assessed using an optical microscope as well as element mapping from the scanning electron microscope. The mineralogy is not complex and consists mainly of calcite, dolomite, quartz, and minor pyrite. Texture was assessed visually using both microscopes. Specific factors that were noted were porosity, connectivity of porosity, pre-existing fractures, grain size, and grain boundary relationships. Replacement textures were noted with respect to dolomite and calcite.

Mineralogy was also estimated based on bulk composition and XRF data. Mineralogy was calculated assuming a three component system based on the procedure outlined in Cleven (2008). The system was assumed to be made up of quartz, dolomite and calcite. Many of the samples exhibit minor amounts of sulphides so there is a potential source for error using this method. Mineralogy and rock characteristics are tabulated below in Tables 1 and 2.

2.1.1d Scanning Electron Microscope

Microscopic observations were taken using the Philips XL30 electron microscope with Princeton Gamma-Tech energy dispersion X-ray spectrometer and image analysis systems. It is located in the clean lab in Earth an Ocean Sciences at the University of British Columbia, Vancouver. Samples were imaged using the back scatter electron mode and element maps were created using the spectrometer.

Sample Number	Mass (g)	Average Length (cm)	Average Radius (cm)	Density (g/cm3)	Porosity (%)	Grain Size (microns)
Mt1-5-70%	70.07	5.09	1.26	2.81	1.18	10-20
Mt1-B-40%	70.88	5.09	1.26	2.82	0.82	30-100
Mt2-6-60%	75.46	5.39	1.26	2.82	X	10-30
Mt2-7-55%	71.05	5.09	1.26	2.82	0.17	10-30
Mt2-9-28%	70.05	5.10	1.26	2.79	0.96	n/a
Mt3-14-50%	71.07	5.09	1.26	2.84	0.94	5-30
Mt3-16-20%	69.29	5.09	1.25	2.77	0.72	40-100
Mt3-17	69.46	5.09	1.26	2.78	0.81	n/a

Table 1: Sample Characterization of deformed cores

Sample Number	Quartz %	Dolomite %	Calcite %
Mt1-B-40%*	16.31	40.95	42.75
Mt1-5-70%	10.00	70.00	20.00
Mt2-9-28%*	61.11	27.86	11.02
Mt2-6-60%	30.00	60.00	10.00
Mt2-7-55%	30.00	55.00	15.00
Mt3-14-50%*	26.52	50.22	23.26
Mt3-16-20%	5.00	20.00	75.00
Mt3-17	n/a	n/a	n/a

Table 2: Mineralogy of deformed samples estimated from thin section. *denotes XRF data is available and was used to calculate mineralogy. Note: No thin section was available for Mt3-17.

2.1.2 Individual Member Descriptions

2.1.2a Mt1 Member

Two samples, Mt1-B-40% and Mt1-5-70%, from the Mt1 were deformed during experimentation. Mt1-B-40% was sent for bulk chemical analysis and its silica content was measured at only 6.24 wt. %, the lowest of any sample tested. Bulk chemical analyses results are tabulated in Appendix A. Based on modal analysis of major minerals, Mt1-B-40% contains 42.75% calcite and 40.95% dolomite (Table 2). Modal

quartz mineralogy is relatively low at 16.31%. Grain size ranges from 10-20 microns and grain boundary texture is interlocking (Table 1). Connected porosity measured by helium pycnometry is 0.82% and porosity in thin section is estimated at 3% in the plane of the thin section and is mainly intracrystalline in nature. Mt1-B-40% is also cross cut by a through going vein at 41^{o} to σ_1 (Figure 10). Microcracks are present subparallel to the core axis and are completely infilled with calcite (Figures 10 and 11). Microcracks are not expected to reactivate.

Mt1-5-70% was not sent for bulk chemical analysis but mineralogy was estimated in thin section at 10% quartz, 70% dolomite, and 20% calcite (Table 2). Figure 10 illustrates the disparity in mineralogy between Mt1-B-40% and Mt1-5-70%. Minor sulphides are present in Mt1-5-70% but are not significant. Grain size is coarse and ranges from 30 to 100 microns (Table 1). Oval regions of finer grained materials are disseminated throughout the sample (Figure 11). Grain texture is euhedral to subhedral. Connected porosity was measured at 1.18% and porosity in the plane of the thin section is estimated at 5%. Porosity is intracrystalline.

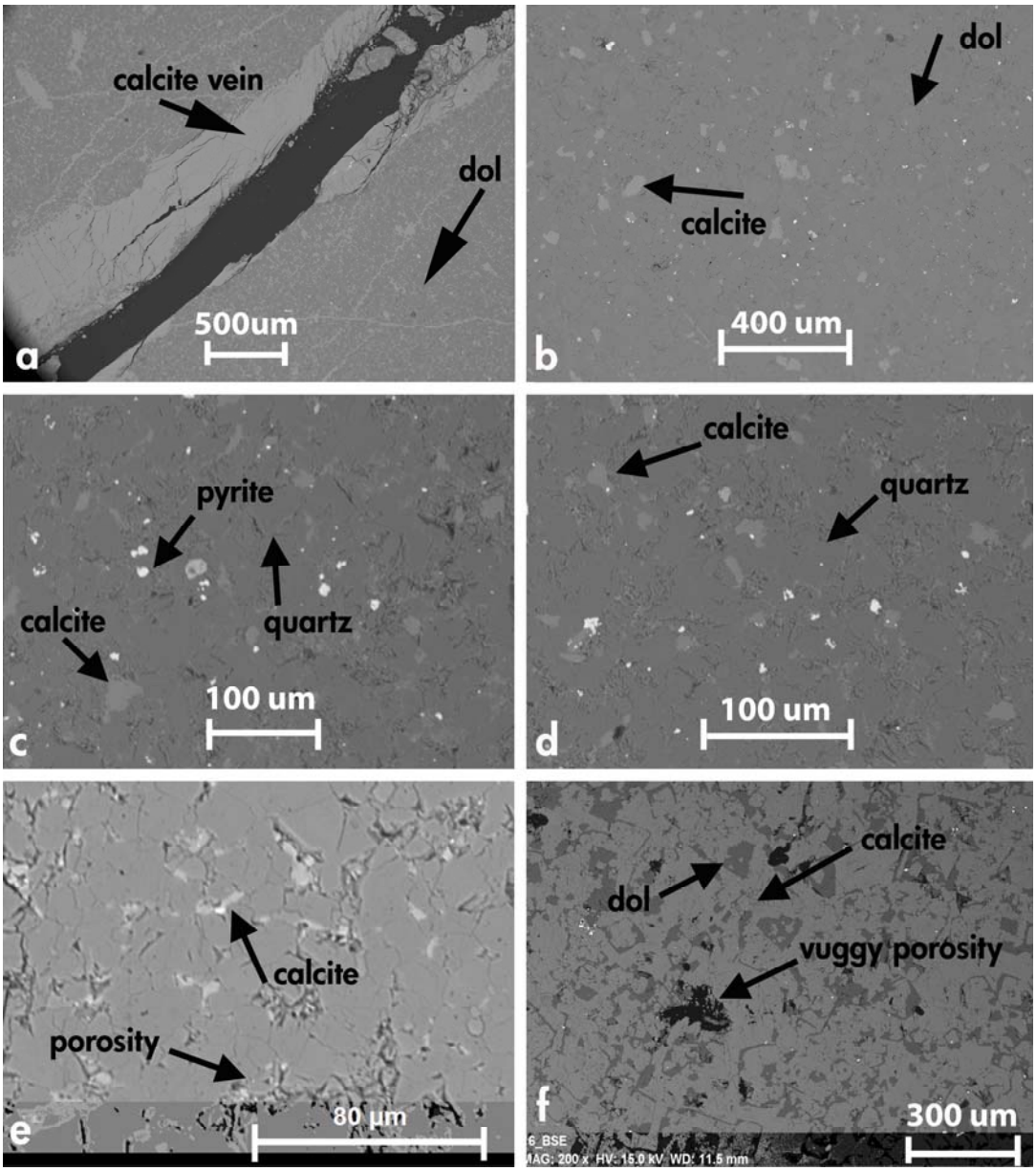

Figure 10: Undeformed material. a) Mt1-B-40%. Note infilled calcite veins in wall rock and major through going vein. This image is post deformation but all calcite filled veins are pre existing. Light material is calcite and dark is dolomite. b) Mt1-5-70% starting material illustrating dolomite to calcite ratio and grain size. c) Mt2-6-60% starting material. Background material is dolomite and grey grains with relief are quartz. d) Mt2-7-55% starting material. Background material is dolomite and grains with relief are quartz. e) Mt3-14-50% starting material, note euhedral grains. Background material is dolomite. f) Mt3-16-20% starting material, note porosity and interlocking texture.

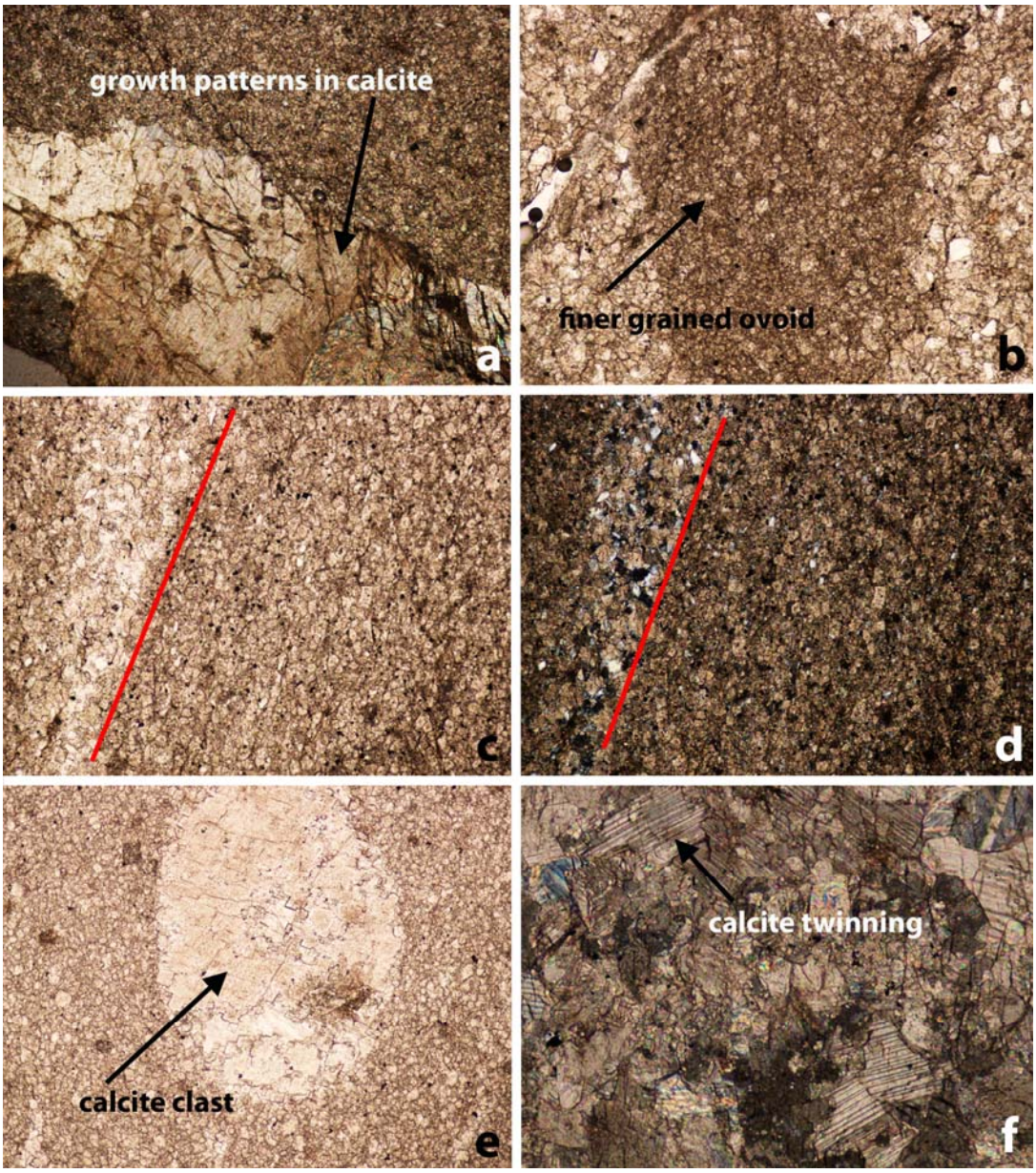

Figure 11: Optical microscope images of starting material. All photos 10X magnification.: a) Mt1-B-40%: highlight of calcite vein in which deformation took place. Growth patterns within the vein are visible. b) Mt1-5-70%: Finer grained ovoid area visible is representative of textural irregularities in the sample. c) Mt2-6-60%: Plane polarized light highlighting the bedding (red line) within the sample. d) Mt2-6-60%: Cross polarized light showing the concentration of quartz along select bedding surfaces, highlighted by red line. Quartz appears grey and black in xpl while carbonates appear brown. e) Mt3-14-50%: Large recrystalized crinoid in sample which may affect strength. f) Mt3-16-20%: Twinning in calcite grains highlighted in cross polarized light illustrating high calcite content within sample.

2.1.2b Mt2 Member

Three samples from the Mt2, Mt2-6-60%, Mt2-7-55%, and Mt2-9-28%, were deformed. Mt2-9-28% was sent for bulk chemical analysis and has the highest SiO_2 content of any rocks in the sample suite (Table 2). Mineralogy was calculated to be 61% quartz, 28% dolomite, and 11% calcite (Table 2). Thin sections were not made for this sample so no grain size estimate could be made. Connected porosity was determined to be 0.96%. No hand sample scale textural heterogeneities are evident.

Mineralogy for Mt2-6-60% was estimated in thin section to be 60% dolomite, 10% calcite and 30% quartz (Table 2). Quartz content is consistently high in the Mt2 (Figure 12). Sulphide grains are disseminated throughout but are not expected to affect mechanical strength. Grain size ranges from 10-30 microns and grains are subhedral to anhedral in appearance (Table 1). An error occurred which prevented connected porosity calculations for Mt2-6-60% but the sample is from the same sample locality as Mt2-7-55% and is expected to have a similar low connected porosity. Prominent bedding planes are present at 20^{o} to the long axis of the core and are defined by slight colour changes and concentrations of quartz in some places (Figure 11). Bedding planes represent planes of weakness and will likely affect rock strength.

Mt2-7-55% is mineralogically and texturally similar to Mt2-6-60%. Mineralogy was estimated from thin section to be 55% dolomite, 30% quartz and 15% calcite (Figure 12). Grain size was estimated at 10-30 microns and connected porosity was calculated at 0.17% (Table 1). Bedding planes are present in this sample as in Mt2-6-60% but are slightly less pronounces and quartz is not as clearly concentrated along bedding planes. Stylolites were observed in both samples subparallel to the short axis of the core. Stylolites are not oriented favourably and are not expected to affect rock strength.

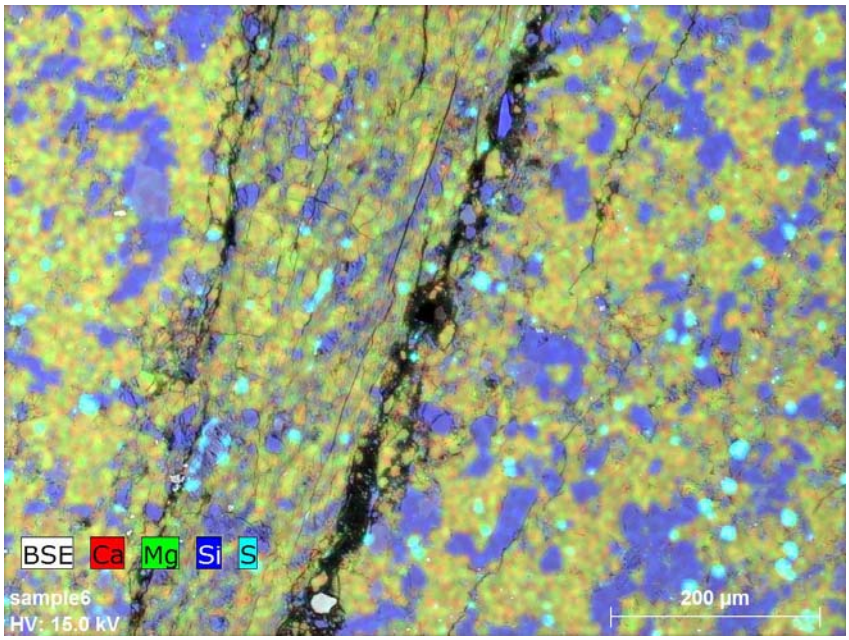

Figure 12: Element map of Mt2-7-55% from Mt2 from the scanning electron microscope. Silica is highlighted in dark blue, indicating quartz in these areas of the thin section.

2.1.2c Mt3 Member

Three samples, Mt3-17, Mt3-14-50%, and Mt3-16-20%, were deformed. A thin section for Mt3-17 was not made so mineralogical and grain size estimates could not be made for this sample. It is evident from hand sample that Mt3-17 is calcite rich. A 2cm diameter fossil is also present in the center of the core. Mt3-14-50% was sent for bulk chemical analysis and modal mineralogy was calculated to be 50% dolomite, 27% quartz and 23% calcite (Table 2). Grain size is estimated to be 5-30 microns and grains are strongly euhedral (Figure 10). Connected porosity was measured at 0.94% and porosity in the plane of the thin section was estimated to be 5% (Table 1). Minor vuggy porosity is visible in hand sample. In general, the sample is texturally consistent but large calcite grains inferred to be recrystalized fossils are present throughout the sample (Figure 11).

Mineralogy estimated from thin section for Mt3-16-20% is 20% dolomite, 5% quartz, and 75% calcite (Table 2). Grain size is estimated to be between 40 and 100 microns and grain boundaries are strongly interlocking (Table 1). Connected porosity

was calculated to be 0.72%. Porosity is vuggy and intragranular in nature within the sample. Dolomite replacement in the sample occurs along the outside of calcite grains (Figure 10). Mt3-16-20% is expected to perform very differently from Mt3-14-50% in rock deformation experiments.

2.2 Experiments

2.2.1 Apparatus

The large sample rig (Figure 13), located at the Center for Experimental Studies of the Lithosphere (CESL) at the University of British Columbia is a triaxial rock press that uses argon gas as a confining pressure system. Confining pressures can be raised up to 100 MPa. Displacement and load are generated by an electric motor gear system that reaches a maximum load of 200,000 pounds. A Saginaw ball bearing screw raises the confining vessel into contact with the upper plate and applies the load to the sample assembly at a fixed displacement rate of 2×10^{-4} cm/s. An external displacement transducer measures displacement and transmits the data to the Lab view program which then converts the electrical signal in milli Volts to displacement in millimetres. Data is collected approximately every 0.6 seconds. Progress throughout the experiment can be observed on the Lab view interface (Cleven, 2008).

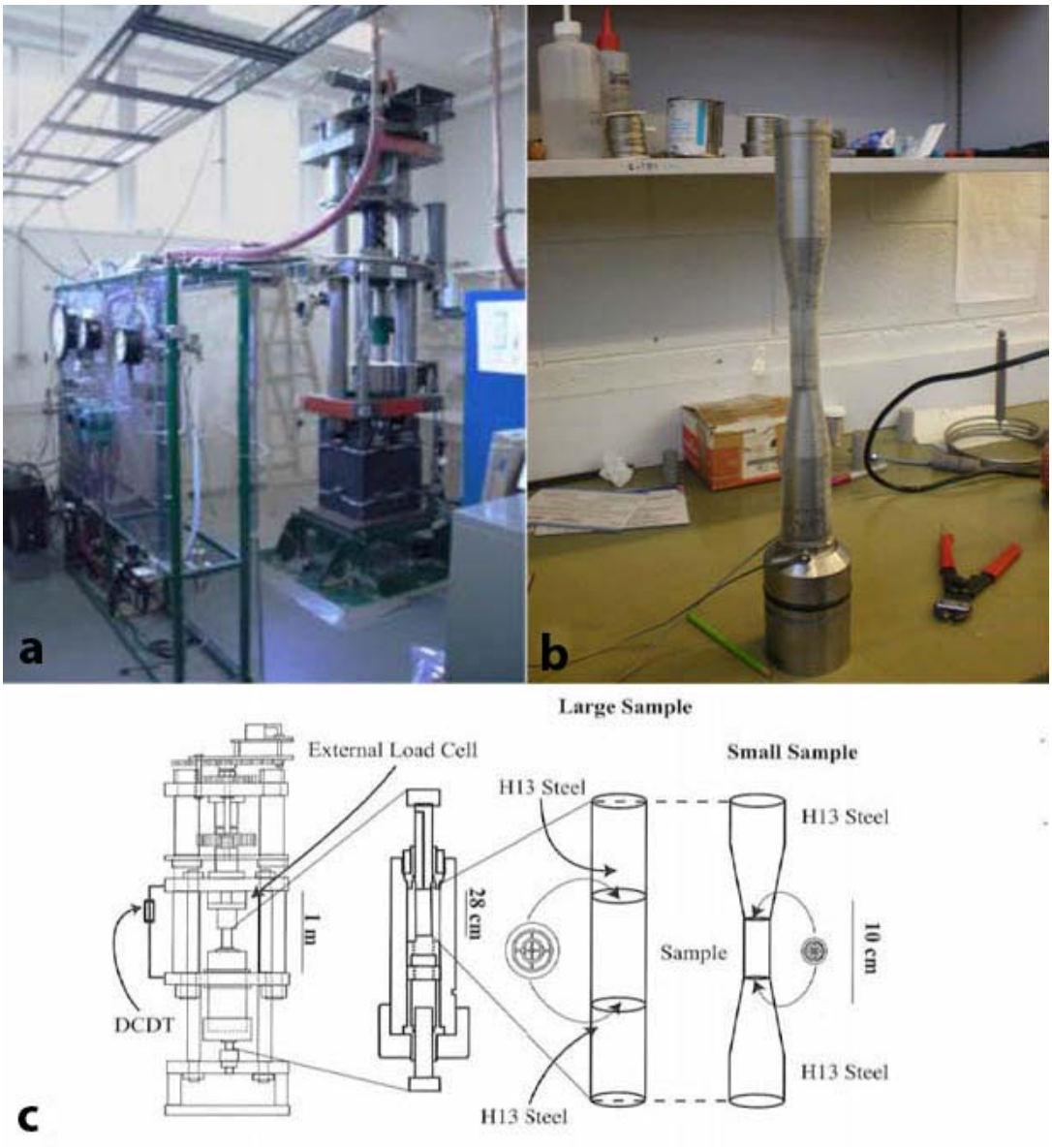

Figure 13: a) The LSR located in CESL. Modified from Cleven (2008). b) Small sample assembly. Polyolefin jacket encases the entire assembly and is sealed by wire at each end. c) Schematic of the LSR (Austin et. al., 2005).

2.2.2 Sample preparation

Samples are cored with a 1 inch diameter drill bit and cut to a length of 2 inches in order to produce a 2:1 length to width ratio. Cylindrical samples are then ground to within one thousandth of an inch to ensure ends are flat. Samples were dried at 100^{o}C overnight and then placed in a desiccator for twelve hours in order to fully dry the

samples. The cooled samples were weighed three times and length and diameter were each measured ten times to ensure accuracy. A helium pycnometer was used to accurately measure the volume of each sample. Porosity and density were calculated from this data. Results are tabulated in Table 1.

2.2.3 Sample assembly

The prepared cores are placed between 1 inch diameter spacers in between upper and lower piston cups (Figure 13). The entire assembly is then secured in polyolefin shrink wrap in order to prevent the argon from accessing porosity in the sample. The ends of the polyolefin wrap are secured with wire to further prevent leakage and the development of unwanted pore pressure. Argon has been shown to infiltrate the polyolefin wrapping but at the time scale of the experiments leakage is not significant (Cleven, 2008).

2.2.4 Experimental grid

The mechanical behaviour of eight select samples of the Mississippian Turner Valley Formation was determined. Samples were deformed under a variety of confining pressures at 798 K and a nominal strain rate of $10^{-4}s^{-1}$. Experiments were run at constant strain rate until a significant drop in load was recorded by the Lab view program, generally accompanied by a loud acoustic emission. Thin sections of deformed rocks were observed using optical and SEM microscopes. Yield strength, peak strength, and strain were calculated from experimental results using the procedure outlined in Cleven (2008). The experimental grid is outlined in Table 3. Confining pressures of 25, 50, and 75 MPa were chosen in order to approximate 1, 2, and 3 kilometres depth in the subsurface.

Sample Number	Rock Unit	Confining Pressure (MPa)
Mt1-B-40%	Mt1	50
Mt1-5-70%	Mt1	25
Mt2-6-60%	Mt2	50
Mt2-7-55%	Mt2	25
Mt2-9-28%	Mt2	75
Mt3-14- 50%	Mt3	50
Mt3-16-20%	Mt3	25
Mt3-17	Mt3	50

Table 3: Experimental grid for deformation experiments

3.0 EXPERIMENTAL RESULTS

3.1 Mechanical Results

The peak and yield strength for all samples are presented in Table 4. Yield strength was determined by isolating the linear portion of the stress strain curve. Yield strength is the point at which the relationship between stress and strain is no longer linear. It represents the point at which microcracking begins (Van der Pluijm and Marshak, 2003). Peak strength was recorded from the maximum load reached by the rock before failure. Displacement was tabulated from the total displacement at the time of failure. Samples for the Mt3 and Mt2 show a general increase in peak strength with increasing confining pressure. Samples from Mt1 did not follow this trend. All samples suites were variable in their textural and mineralogical properties and this is reflected in the results. At 25 MPa confining pressure, Mt3-16-20% from Mt3 was the weakest (Figure 14). At 50 MPa, Mt3-14-50% from the Mt3 was by far the strongest rock and Mt3-17, also from Mt3, was the weakest (Figure 14). Other inconsistencies in rock strength were noted throughout experimentation and will be discussed.

Sample Number	Confining Pressure (Mpa)	Yield Strength (Mpa)	Peak Strength (Mpa)	Displacement (mm)
Mt1-B-40%	25	604.90	611.30	0.10
Mt1-5-70%	50	446.20	446.20	0.08
Mt2-6-60%	50	475.03	475.03	0.09
Mt2-7-55%	25	415.86	426.51	0.07
Mt2-9-28%	75	670.80	759.30	0.12
Mt3-14- 50%	50	602.43	646.80	0.10
Mt3-16-20%	25	265.72	288.82	0.06
Mt3-17	50	314.33	361.72	0.08

Table 4: Summary of experimental rock deformation results for Mtv, Displacement represents total displacement during experiment.

a)

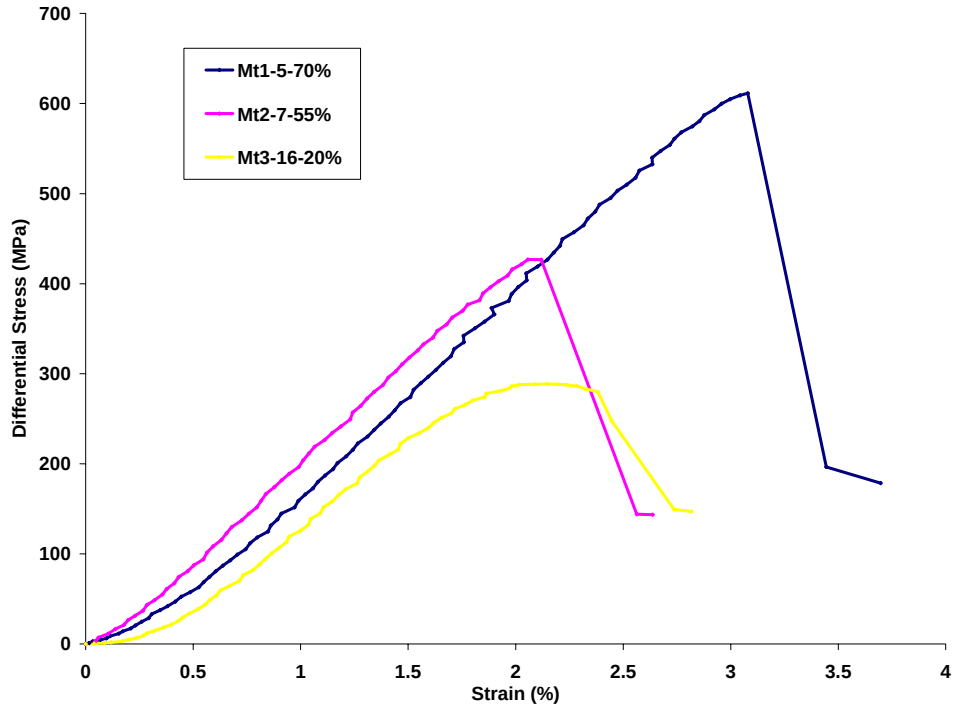

b)

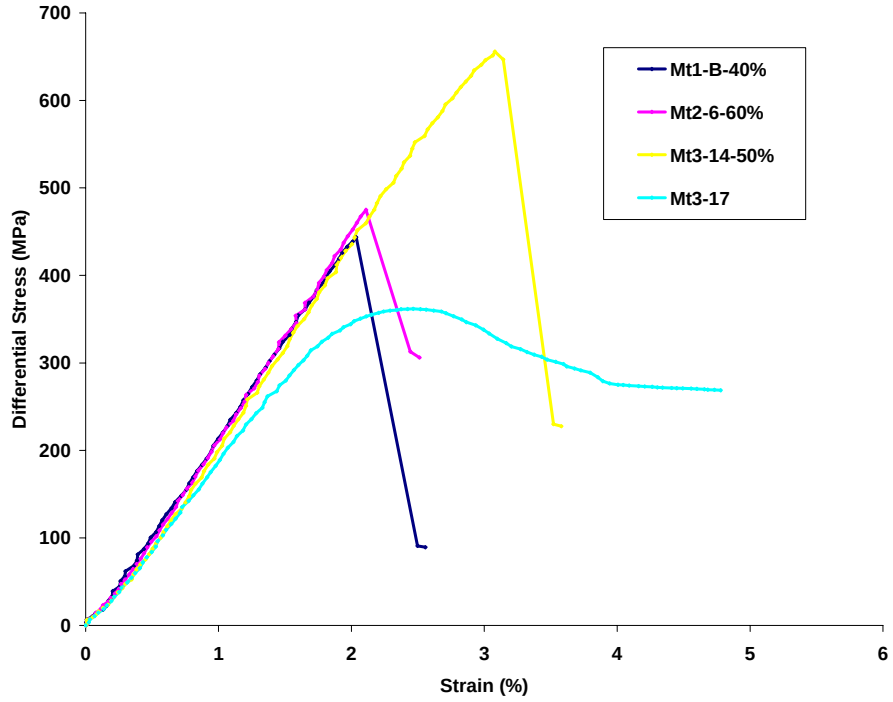

Figure 14: Stress strain curves for experiments conducted at a) 25 MPa and b) 50 MPa confining pressure.

The large amount of heterogeneity in results precluded the construction of failure envelopes for the Mt1. In the Mt2, bedding plane weaknesses resulted in variable data but as Figure 15 shows, a failure envelope can be calculated from results for Mt2-7-55% and Mt2-9-28%. Mt2-6-60% and Mt2-7-55% failed primarily on bedding planes while Mt2-9-28% did not have pronounced bedding surfaces. As a consequence, the failure envelope may not be representative of the entire Mt2 unit.

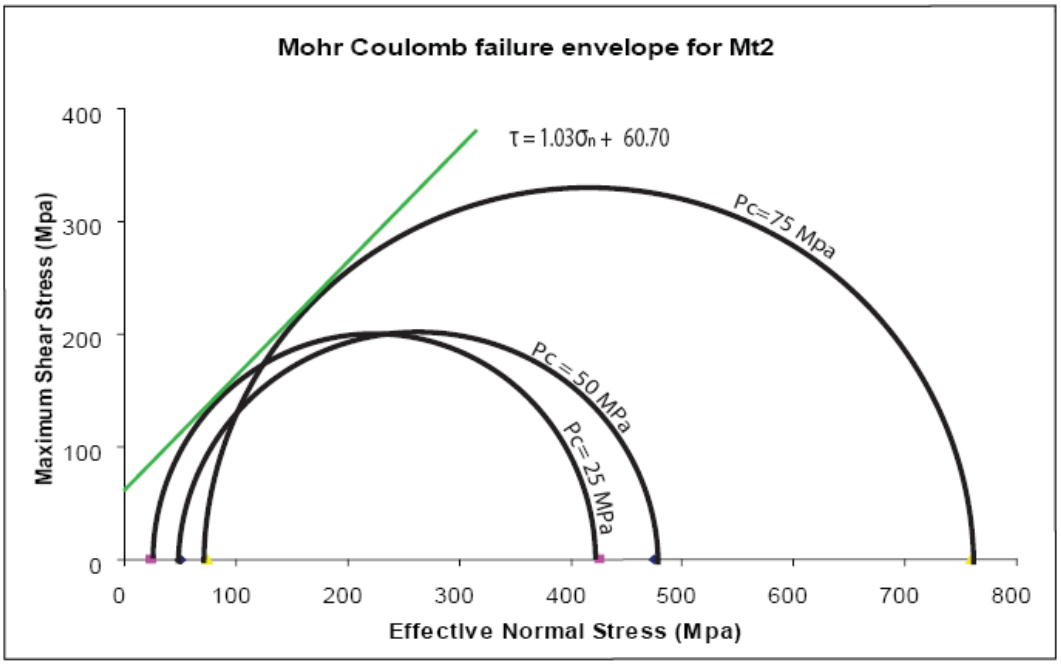

Figure 15: Mohr Coulomb failure envelope for the Mt2.

The failure envelope for the Mt3 member was created using results from Mt3-16-20% and Mt3-17. Mt3-16-20% and Mt3-17 can be assumed to be comparable as they are from the same depth on the core, though they may not be representative of the entire Mt3.

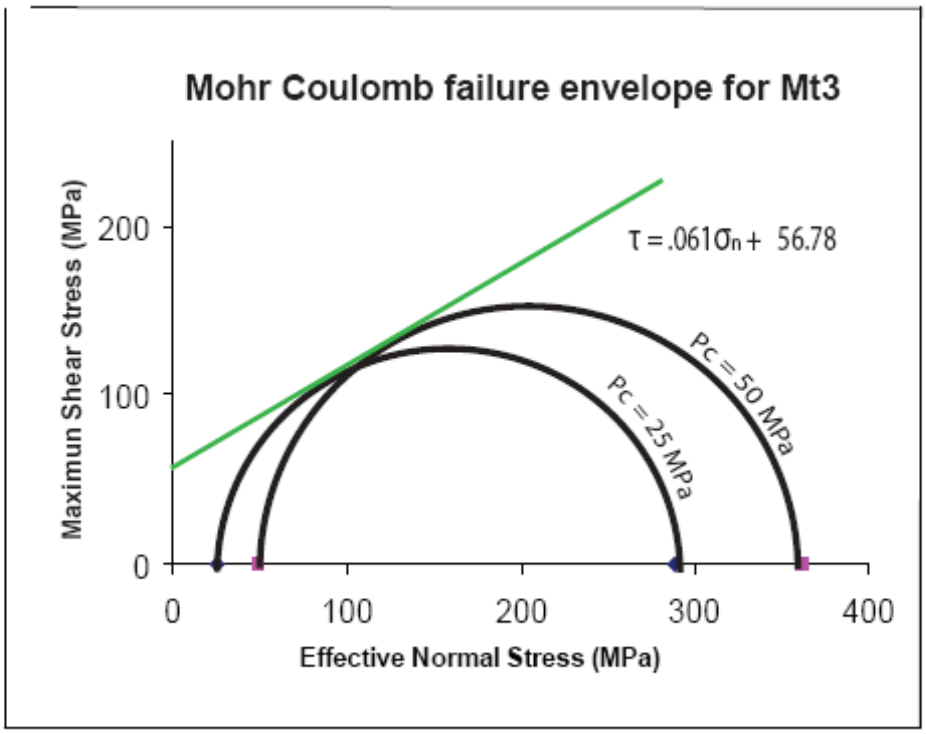

Figure 16: Mohr Coulomb failure envelope for the Mt3. Results from Mt3-16-20% and Mt3-17 are used.

3.2 Macroscopic and Microscopic Observations

3.2.1 Macroscopic Observations

For all run products, fracture zone thicknesses were measured and photographed. Angles and widths of fracture zones are tabulated below in Table 5. There was a great deal of variability in fracture morphology between samples which is representative of variability within the sample suite.

3.2.1a Mt1 Member

In the Mt1, Mt1-B-40% fractured along a pre-existing favourably oriented calcite filled vein. The fracture network in Mt1-5-70% was the most complex pattern observed (Table 5). Due to the variability in results, a failure envelope could not be constructed for the Mt1. Neither sample exhibited ductile behaviour during deformation (Figure 14). Yield strength and peak strength were similar to each other in Mt1-5-70% and identical in Mt1-B-40%, indicating that failure and first microcracking were nearly instantaneous. This is likely due to the weak calcite vein oriented 41^{o} from the long axis of the core. Deformation was completely isolated to the calcite vein (Figure 17).

The fracture network in Mt1-5-70% was extensive and complex, involving over a third of the core (Table 5). Mode 1 cracks in the deformed sample coalesce to form a through going fracture zone. No single main fracture is present. Yield strength and peak strength differ by only 6 MPa in this sample which indicates that response was elastic nearly to the point of failure. Mt1-5-70% exhibits a bulged appearance (Figure 17). Mechanical results show that this is not due to ductile deformation and is likely the result of the diffuse nature of the fracture network.

3.2.1b Mt2 Member

Fracturing in the Mt2 was strongly controlled by bedding, where present in Mt2-6-60% and Mt2-7-55%. Fractures occur completely along bedding in Mt2-6-60% and partially along bedding in Mt2-7-55% (Table 5, Figure 17). Fracture thicknesses were less that 1 millimetre in both samples. In both samples, yield strength did not markedly differ from peak strength indicating that minimal ductile deformation occurred.

Bedding was not well developed in Mt2-9-28% and did not affect fracture morphology. Yield strength differs from peak strength by 90 MPa in this sample but overall, deformation occurs in the brittle field (Table 4). Mt2-9-28% also exhibited a wider fracture zone ranging in size from 1-3 millimetres (Table 5). A failure envelope for the Mt2 was constructed using samples Mt2-9-28% and Mt2-7-55% (Figure 15). Due

to the heterogeneities in fracture style, this failure envelope may not be representative of the entire Mt2. Failure style will depend on the orientation of stresses with respect to bedding within the unit.

Sample Number	Fracture Angle (from σ_1)	Fracture Zone Thickness (mm)	Notes
Mt1-5-70%	X	13.75	Fracture network too complex to measure
Mt1-B-40%	41	1.2	Fracture occurred along existing vein
Mt2-6-60%	17	0.25	Fractured along bedding plane
Mt2-7-55%	7,10	<1.00	Two conjugate fractures
Mt2-9-28%	27	1-3	1 major through-going fracture with smaller associated fractures
Mt3-14- 50%	14	0.75	1 major through going fracture
Mt3-16-20%	20	0.75	1 major through going fracture with splays at ends of core

Table 5: Macroscopic observations of fractured samples

3.2.1c Mt3 Member

Samples from the Mt3 behaved the most consistently on a macroscopic level and both Mt3-14-50% and Mt3-16-20% failed along one major through going fracture with a thickness of 0.75 millimetres. Figure 17 illustrates end member failure styles observed in hand sample. An error was made while running the experiment for Mt3-17. While mechanical results are still valid, fracture thickness measurements could not be taken due to crushing of the sample. Mt3-17 and Mt3-16-20% both deformed ductily (Figure 14) in deformation experiments and are very calcite rich. No failure occurred in Mt3-17 and

brittle failure occurred after a long period of ductile deformation in Mt3-16-20%. Mt3-14-50% behaved very differently and was compositionally very different. Dolomite content in Mt3-14-50% is significantly higher and behaviour during deformation was strongly brittle. One major discrete fracture crosscuts Mt3-14-50%.

Mt3-16-20% and Mt3-17 were chosen to construct a failure envelope (Figure 16) as their behaviour was considered to be the most consistent. Variability between Mt3a, b, and c means that these two units will not be representative of the entire Mt3 but will provide a good experimental analogue for calcite rich regions of the Mt3 unit.

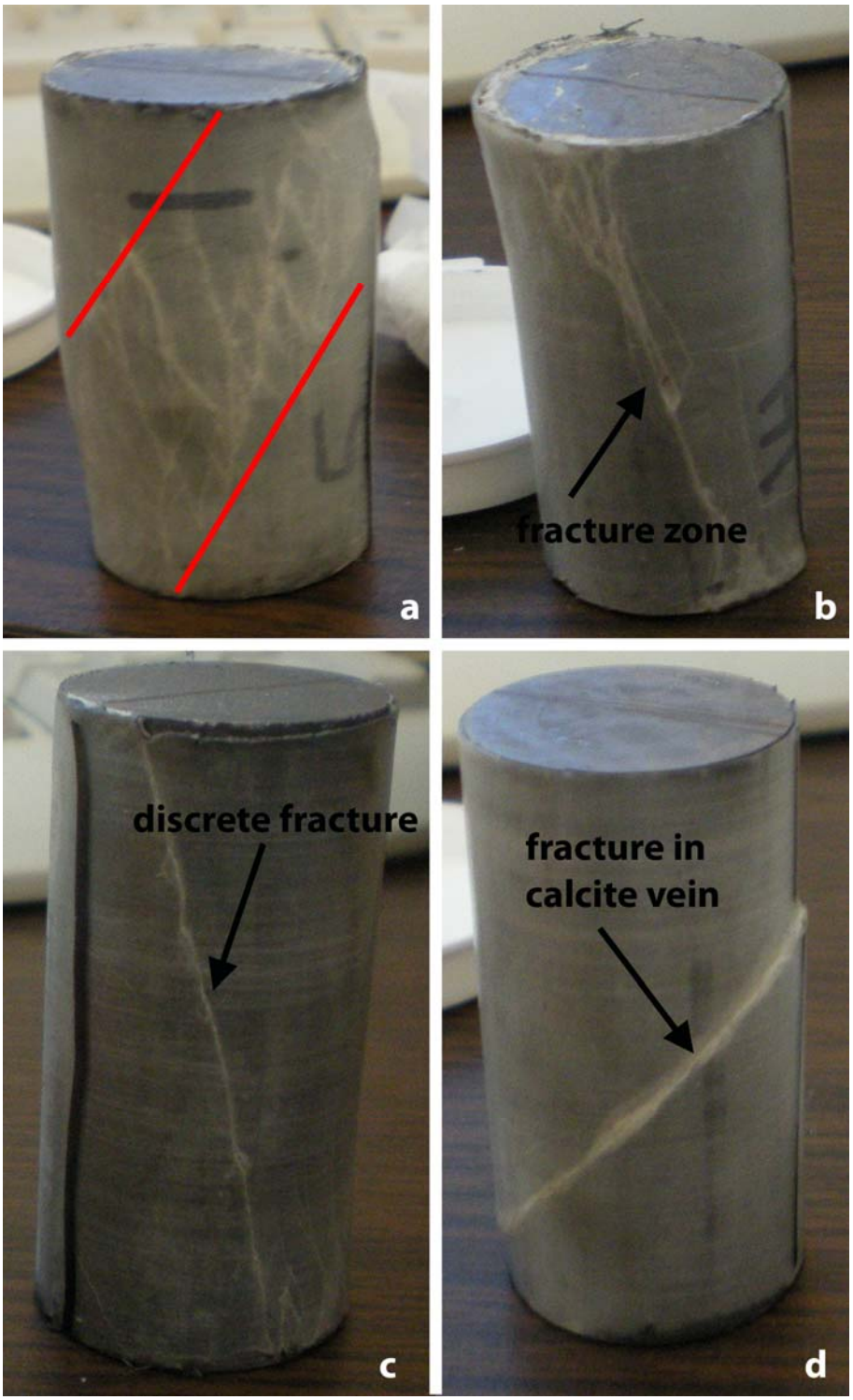

Figure 17: Core samples after experimentation. All samples are 5.08 cm by 2.54 cm. a) Mt1-5-70%, most complex fracture network observed, highlighted by red lines. b) Mt3-14-50%, one major through going fracture with splays at fracture terminations. c) Mt2-6-60%, clean fracture along bedding plane. d) Mt1-B-40%, fracture along pre-existing bedding plane.

3.2.2 Microscopic Observations

Because of the fine grain size of samples, the scanning electron microscope in back scatter electron (BSE) mode was used to image fault and damage zones. An optical microscope was also used to observe samples and results are tabulated below by unit. Microscopic responses to stress were variable within units and between units.

3.2.2a Mt1 Member

Mt1 represents a highly dolomitized unit. Mt1-5-70% has the highest dolomite content of any sample in the suite. The sample is 70% dolomite and calcite makes up only 20%. Quartz makes up the remainder. It is very fine grained with grain sizes ranging from 10-20 microns. Mt1-5-70% exhibited a very diffuse fracture network encompassing over a third of the core volume. Fractures appear to be a wide zone of coalescing mode 1 fractures intersected by failed stylolite planes (Figure 18). Deformation was accommodated both along grain boundaries and by intragranular deformation. Grain size reduction in this sample results in single crystal gouge ranging in size from 1 to 50 microns with larger clasts consisting of multiple grains present as well (Figure 18). The gouge is very angular as is present throughout the fracture network. More drastic grain size reduction is evident in zones where multiple fractures have coalesced into one (Figure 18). Wall rock deformation consists mostly of mode 1 cracks along grain boundaries with some fracturing along previously developed mechanical twinning. Deformation is accommodated in both dolomite and quartz grains and along their boundaries (Figure 18). Fractures within quartz grains exhibit concoidial morphology while fractures within dolomite are linear. No new twinning is evident in minimal calcite present but due to the fine grain size, it is difficult to observe individual grains in cross polarized light.

In some sections of Mt1-5-70%, a local reduction in grain size and increase in porosity is associated with a narrowing of the fractured band and a decrease in the

amount of grain size reduction. Deformation in these areas is predominantly along grain boundaries. The reduced grain size does not reflect the dominant texture in the sample.

Mt1-B-40% is cross cut by a large calcite vein oriented 41^{o} from the long axis of the core. Mineralogy is approximately 40% dolomite, 40% calcite and 16% quartz. Grain size ranges from 30-100 microns in the groundmass. Deformation in Mt1-B-40% is almost exclusively accommodated within the pre-existing calcite vein at 41^{o} to σ_1. Areas in which the vein thins drastically allow deformation to step out into the dolomitic sidewall but this is rare (Figure 18). Deformation within the calcite vein does not occur along crystal growth patterns within the vein (Figure 11). Grain size reduction within the calcite vein is drastic and individual particles are too small to be measured. Significant amounts of gouge were inadvertently removed during the thin sectioning process so remaining gouge may not be completely representative.

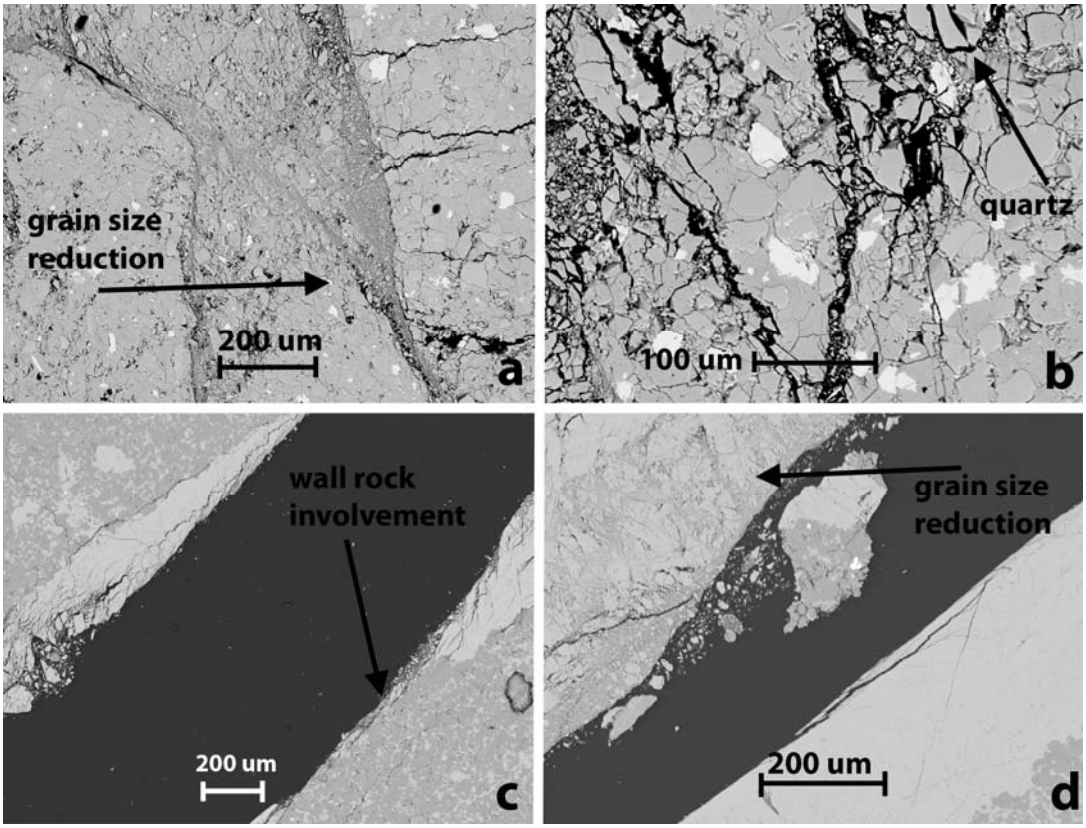

Figure 18: SEM images from the Mt1 member. a) Mt1-5-70%: Electron photomicrograph highlighting increased grain size reduction as fractures coalesce. b) Mt1-5-70%: close up of deformation in Mt1-5-70% highlighting the intragranular fractures and grain boundary deformation styles. Concoidial fracturing in quartz is highlighted. c) Mt1-B-40%: Fracture area where dolomite has been slightly involved in deformation at a thinning of the calcite vein. d) Mt1-B-40%: Extreme grain size reduction in calcite in the vein. Note the deformation in the calcite does not follow pre-existing cleavage patterns (Figure 11).

3.2.2b Mt2 Member

Thin sections were made for Mt2-6-60% and Mt2-7-55%. Mt2-6-60% and Mt2-7-55% contain about 30% disseminated silica and are very fine grained. Grains range in size from 10 to 30 microns. In both samples, the main fracture occurs along pre-existing bedding planes representing favourably oriented planes of weakness at about 10-15^{o} from σ_1 (Figure 11). Mt2-6-60% fractured cleanly along one bedding plane and the entire fracture exhibits very linear and parallel edges (Figure 19). The majority of gouge has

been lost in the thin section process but Figure 19 illustrates that grain size reduction occurred along the fracture surface. Gouge is too fine to be measured. Regions outside of the main fracture zone are generally undeformed but where small fractures exist they are parallel to the main fracture zone and consistent with bedding. Deformation is accommodated both along grain boundaries and within grains. Mode 1 cracks are rare outside of the fracture zone. Deformation is almost completely isolated to the fracture zone. Calcite content is low and grain size is very small and consequently twinning was not observed.

The major fracture in Mt2-7-55% occurs along bedding in the centre of the sample but fracture patterns are disseminated at the ends of the sample. Within the zone that deformed along bedding, fracture zone boundaries are extremely linear and large clasts are present in the gouge as well as well as grains too small to be measured. Deformation is primarily along grain boundaries but occurs intragranularly as highlighted by grain size reduction in Figure 19c. Fracturing outside of the linear central fracture zone exhibits a Riedel fabric and grain size reduction is more pronounced (Figure 19). Some fractures terminate or step over along stylolites within the sample. Mode 1 cracks are present outside of the main fracture zone but wall rock deformation is not pronounced in the sample.

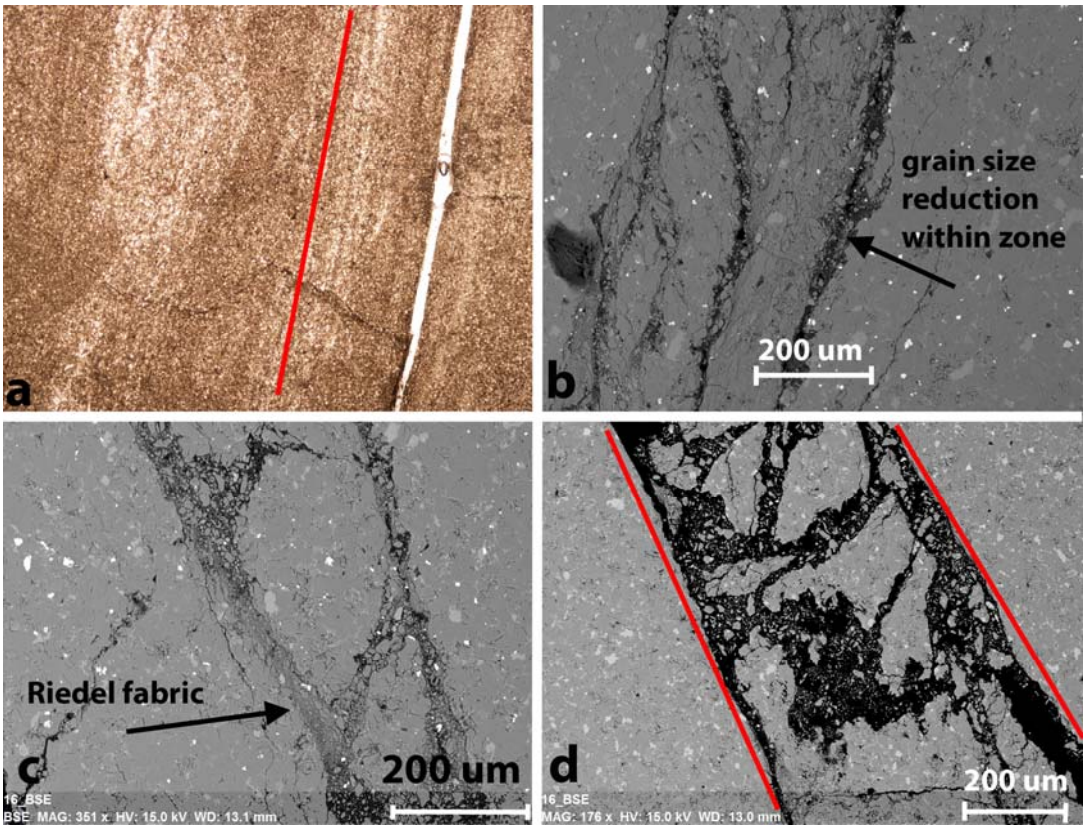

Figure 19: SEM images from the Mt2 member. a) Optical microscope image (2X magnification) of fracturing along bedding in Mt2-6-60%. Bedding is highlighted in red. ii) Electron micrograph of fracture zone in Mt2-6-60%. Note extremely linear fracture zone terminations defined by bedding and grain size reduction within the fracture zone. iii) Electron micrograph of Mt2-7-55%. Note wider deformation zone and development of Riedel fabric. iv) Mt2-7-55% electron micrograph. Note linear fracture zone boundaries. Main fracture defined by bedding.

3.2.2c Mt3 Member

Thin sections were made from Mt3-16-20% and Mt3-14-50% in the Mt3. Mineralogically and texturally, Mt3-14-50% and Mt3-16-20% are extremely different and this is represented in fracture morphology. Mt3-14-50% is highly dolomitic and grains are predominantly euhedral. Fractures are diffuse and deformation occurs along grain boundaries. Mode I cracks are extensive throughout the sample. Grain size reduction occurs but is limited and the smallest grains are greater than 1 micron across (Figure 20). Large calcite clasts inferred to be relict fossils are present and small fractures

terminate or dissipate upon interaction with these clasts (Figure 20). Calcite content is minimal and consequently twinning is not noted throughout the sample. Weak twinning is present in some large calcite clasts but the majority of strain is accommodated by the dolomite.

Mt3-16-20% consists of significantly higher calcite content, minimal quartz, and grains exhibit a strongly interlocking texture (Figure 20) Grain size reduction is extreme and small grains are no longer decipherable from one another at the range of magnification of the scanning electron microscope. Cataclastic flow has occurred within the fracture zone and the width of the deformation area is significantly smaller than Mt3-14-50% (Figure 20). Twinning is pronounced and deformation occurs primarily intragranularly. Breakages occur along twins (Figure 20). Wall rock deformation is made up of diffuse mode 1 cracks within 2 millimetres of the main fracture.

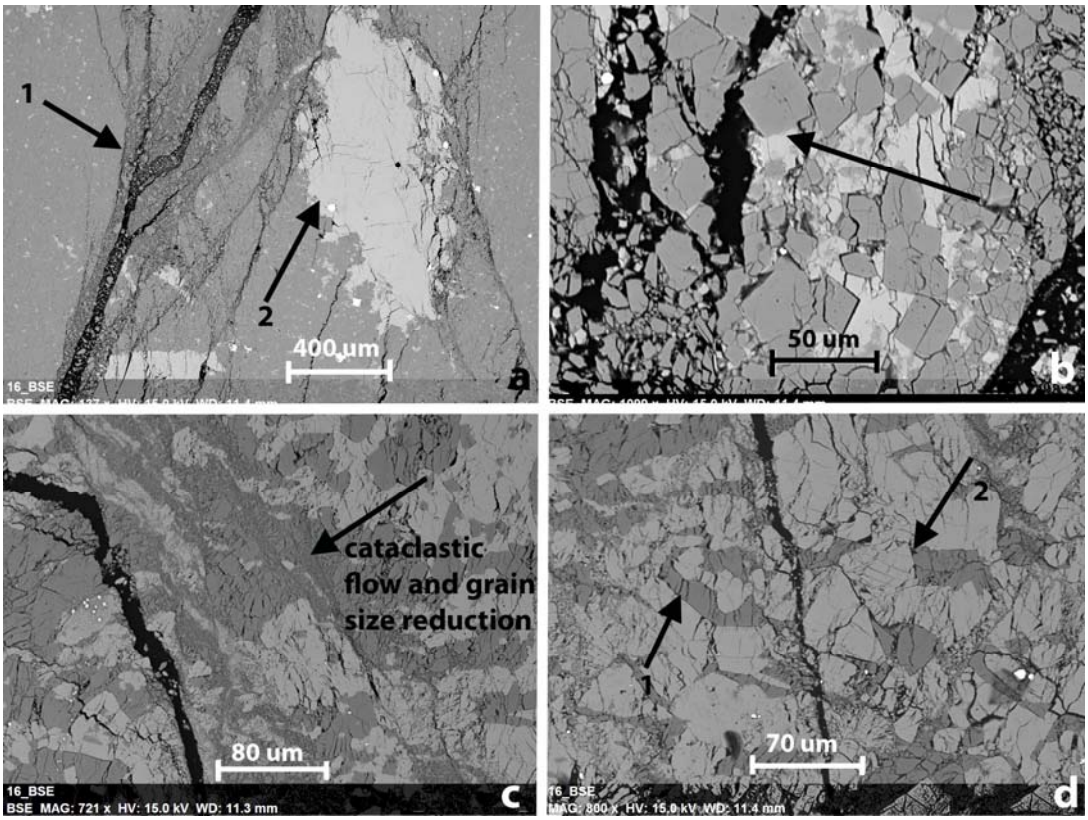

Figure 20: SEM images from the Mt3 member. a) Mt3-14-50%, diffuse fracture zone interacting with relict fossils replaced by calcite. 1 indicates part of main fracture network and 2 indicates a large calcite clast. ii) Mt3-14-50%, grain boundary slip within the fracture zone. Arrow indicates failure along grain boundaries. iii) Mt3-16-20%, cataclastic flow within the fracture zone. iv) Mt3-16-20%, Intragranular deformation in calcite and dolomite and mechanical twinning in Calcite. 1 indicates interlocking texture and 2 points out intragranular deformation

4.0 INTERPRETATION OF RESULTS

Due to the large degree of heterogeneity between samples, it is difficult to make comparisons between individual samples. Grain size, grain boundary texture, and mineralogy are variable within the sample suite. Pre-existing planes of weakness such as bedding and veins are present in some samples. This heterogeneity is reflected in the data. In the Mt1 series Mt1-B-40% was deformed at 50 MPa confining pressured and reached a peak strength of 446.2 MPa while Mt1-2-70% was deformed at 25 MPa and reached a peak strength of 611.3 MPa. Increased confining pressure typically increases rock strength. Macroscopic sample analysis showed that Mt1-B-40% failed along an existing plane of weakness. A 1 to 2 mm wide calcite vein oriented at 41^{o} from σ_1 cross cuts the sample and failure occurs almost exclusively along this plane of weakness. No such through going plane of weakness exists in Mt1-5-70% and it is therefore mechanically stronger.

In the Mt2 series a general increase in strength with increasing confining pressure was noted and a Mohr Coulomb failure envelope was created for the Mt2. Well defined bedding was present in Mt2-6-60% and Mt2-7-55%, though bedding in Mt2-7-55% is wavier in nature. Both samples were from the same location in the core. Mt2-6-60% was deformed at a confining pressure of 50 MPa and Mt2-7-55% at 25 MPa. The difference in peak strength between the two samples was only 29 MPa. Mt2-6-60% failed cleanly along a plane of weakness defined by bedding while Mt2-7-55% did not completely fail along bedding. The variability in failure morphology is inferred to be the reason for the minimal increase in rock strength as confining pressure increased from 25 to 50 MPa. Mt2-9-28%, deformed at a confining pressure of 75 MPa, did not fail along any pre-existing planes of weakness and was significantly stronger.

Samples in the Mt3 show a general strengthening trend with increasing confining pressure. Mt3-16-20% and Mt3-17 are highly calcareous and are comparatively weak rocks. Mt3-14-50% is highly dolomitic and significantly stronger at the same confining pressure as Mt3-17 (50 MPa). A Mohr Coulomb failure envelope was created using results from Mt3-17 and Mt3-16-20% as they are considered to be comparable lithologies while Mt3-14-50% is texturally and mineralogically significantly different. Palchik and

Hatzor (2000) point out that in low porosity samples, grain boundaries will act as original Griffith flaws. Mt3-14-50% exhibits this behaviour and failure occurs along grain boundaries.

Overall, Mt1-5-70% and Mt3-14-50% are the strongest carbonate samples and also the most dolomitic. Sample from the Mt2 are consistently strong when fracturing does not occur along bedding planes which represent significant weaknesses in the rock. Mt3-16-20% and Mt3-17 from the Mt3 are very weak compared to the rest of the sample suite and are also the most calcite rich of the samples. Results are consistent with previous experimental studies. Calcite has been shown to be mechanically weaker than dolomite (Austin et. al., 2005) as is exhibited by the comparative rocks strengths in the Mt3. Finer grained material is generally stronger than coarse grained material (Fredrich et. al., 1990). Samples from the Mt2 are the finest grained and are also consistently strong rocks despite having failed along planes of weakness.

5.0 DISCUSSION

5.1 The Role of Dolomite in Fracture Strength

In the Jumping Pound Reservoir, dolomitization is associated with improved reservoir quality. Dolomitization tends to increase intergranular porosity within carbonates. Dolomite rich carbonates are typically mechanically stronger and tend to generate more fractures with failure. Gaswirth et. al., (2006) found that dolomite was more likely to fracture than limestones and that strength increased with a reduction in porosity. Experimental results are consistent and showed that calcite rich rocks experienced a large amount of ductile deformation prior to failure while dolomitic samples do not (Figure 14). Carbonates with high calcite content exhibited a higher degree of grain size reduction, and fine grained gouge typically lines fractures. The fine grained powder would likely act to inhibit fluid flow. Dolomitic samples generally fractured along grain boundaries and large clasts of wall material were visible within the fracture zone. This morphology increases the potential for gas flow through a fracture because the fault is propped open by clasts of wall rock. This phenomenon is particularly pronounced in the Mt2 and in Mt3-14-50% of the Mt3. Both samples are highly dolomitic. Calcite rich samples such as Mt3-16-20% exhibit extensive grain size reduction and calcite gouge generally fills fracture zones.

5.2 Comparison of Results to Natural Fracturing in the Jumping Pound West Field

Natural fracture data in the Jumping Pound West Reservoir is restricted to FMI logs which record the frequency of fractures but not the type of fracture morphology. In some wells, core is available. Thin section observations from core shows connected networks of fractures rather than individual fractures but information relating to the orientation of thin sections in the subsurface is not available. It is difficult to determine whether the fractures are related to depressurization of the core as it was removed from the subsurface

or natural fracture networks. Due to this informational gap, it is difficult to correlate between natural and experimental data.

The Mt2 is known to act as a baffle (an impermeable layer) to hydrocarbon flow in the subsurface therefore connected fracture networks probably do not exist in the in situ Mt2. Experimental run products of Mt2 cores show that deformation zones in the Mt2 cores tend to be relatively narrow primarily because failure occurred along bedding planes. If strain is accommodated by brittle faulting along bedding surfaces in the subsurface, then an interconnected fracture network is not likely. In addition, porosity is very low in this rock due to its fine grained texture. It is also possible that even with connected natural fractures produced, not enough of the porosity is intersected to allow for the flow of hydrocarbons into the well bore.

The Mt3, specifically the Mt3a member is the major producing unit in the JPW (Eggenkamp, 2007). The Mt3 is also generally highly fractured within Jumping Pound West. FMI and core data show high fracture densities within the Mt3, especially the Mt3a. Fracture density is also generally high within the Mt1. Depending on the well, either the Mt3 or the Mt1 represents the most fractured unit. In the most proximal well with fracture data, Jumping Pound West #37_2, the Mt3a is the most fractured unit as well as the most porous. Permeability data from core samples in the study well is consistent with this trend (Figure 21). Peak horizontal permeability was determined to be located in the Mt3a but significant peaks are also present in the Mt1. High permeability zones correlate with stronger and more dolomitic samples. The strongest cores are from the Mt1 and Mt3 and the highest permeabilities are also in the lower portion of the Mt1 and the upper portion of the Mt3 (Figure 21).

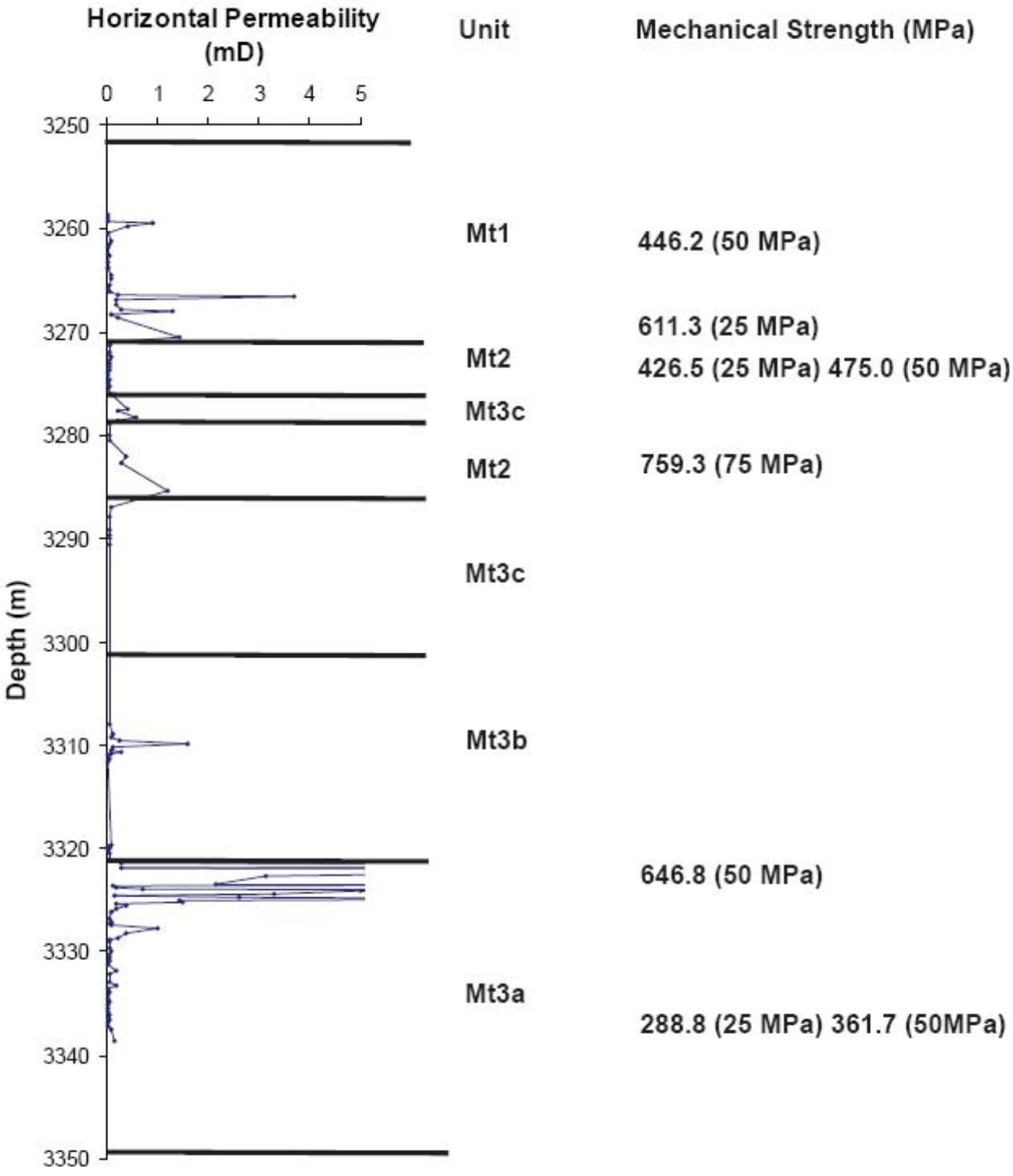

Figure 21: Horizontal permeability vs. mechanical strength. Peak strength is listed with confining pressure in brackets.

Overall, dolomitic textures in the Mississippian Turner Valley tend to be more favourable reservoirs and tend to fracture favourably along grain boundaries. This is consistent with well performance data from the Jumping Pound West field (Figure 21). Limestone units are less favourable reservoirs not only because of their reduced porosity but also because fractures in calcite rich units are less favourable to flow due to the production of fine grained gouge. Mt2 has been shown experimentally to be a mechanically brittle unit. Despite limited grain size reduction, there may not be enough initial porosity for fractures to create a connected network.

Antonellini and Mollema (2000) found that faults with small offsets characterized by en echelon faulting created good connected porosity while areas with a large offset and significant brecciation represented barriers to flow. Observations were at an outcrop scale but structures are analogous to cores. Samples that deformed with limited grain size reduction and a diffuse fracture network (Mt1-5-70% and Mt3-14-50%) are contained in high permeability zones while samples with significant gouge correlate to low permeability zones (Figure 21).

The experimentation conducted leaves large potential for future work. It would be interesting to measure the permeability created by the fracture networks to more quantitatively assess the affect of dolomite content on fracture permeability (eg. Van der Reep, 2009). More samples would be beneficial as well because the reservoir rocks are so variable and the experiments conducted thus far have not been consistent enough to develop conclusive patterns. An experimental suite consisting of buckling experiments with longer length to width ratios would also be interesting as the type of fracture expected to flow in the Jumping Pound West Field are Mode 1 type extensional cracks.

5.3 Implication for Hydrofracturing

Increased understanding of the relationship between texture, porosity, mineralogy, and rock strength will aid in making decisions with respect to well completions. Knowledge of the mechanical strength of the units can permit calculation of the amount of pore pressure that is required to generate hydrofractures. Inducing hydrofractures in

well bores, by increasing pore pressure to exceed σ_3, is very common in the oil and gas industry and is used as a secondary recovery process. Using failure envelopes developed for the Mt2 and Mt3, the pore pressure required to induce fracturing can be determined (Figures 15 and 16). For example, a unit with a peak strength of 400 MPa at 3 km depth would require a minimum pore pressure of 33 MPa in order to induce fracture formation (Figure 22).

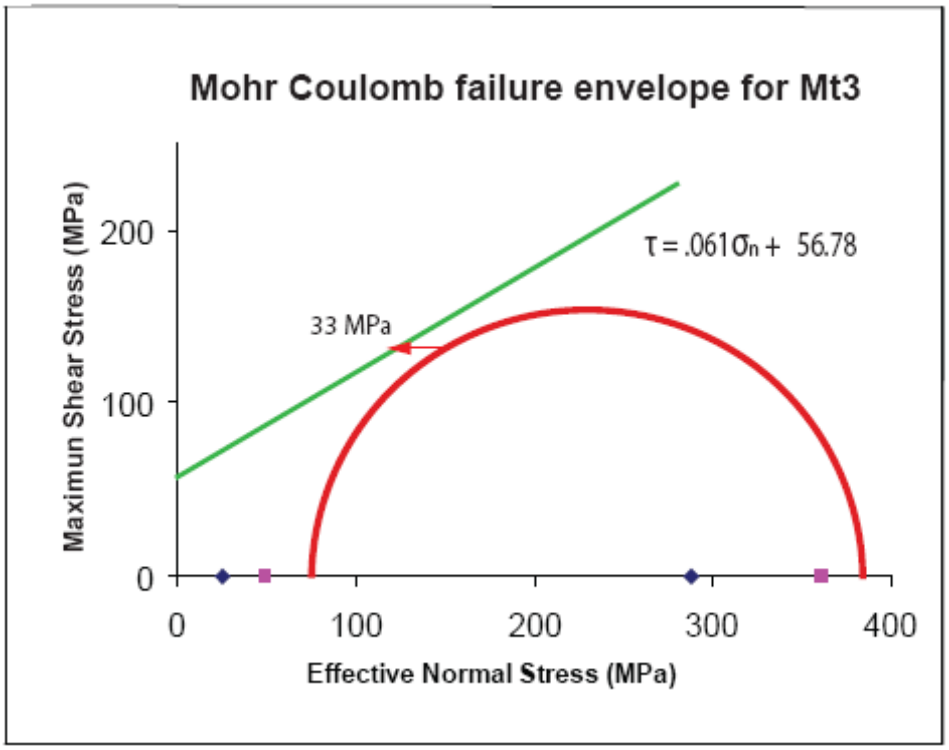

Figure 22: Failure envelope for the Mt3 illustrating the amount of pore pressure required to induce fractures in a rock with a mechanical strength of 400 MPa at 3 km depth.

6.0 CONCLUSION

The large degree of variability in texture, grain size, and lithology within the sample suite makes any patterns in fracture morphology and rock strength difficult to recognize. Overall, dolomitic samples are mechanically stronger than calcite rich samples in the suite and fractures developed in dolomite rich samples are likely more favourable for fluid flow. A larger experimental suite would be extremely beneficial in order to better define rock variability in the reservoir as the limited sample suite cannot be assumed to represent end member textures and mineralogy within the Mississippian Turner Valley in the Jumping Pound West Field. Peak strength in experiments varied from 288.82 MPa to 759.3 MPa illustrating that both texture and mineralogy are extremely variable within the sample suite as in nature. The results of experimentation in this sample suite help to better constrain the relationship between texture, porosity, and mineralogy on the mechanical strength of the units and the fracture morphology in Jumping Pound West.

7.0 REFERENCES CITED

Antonellini, M., and Mollema, P.N., 2000, A Natural Analog for a Fractured and Faulted Reservoir in Dolomite: Triassic Sella Group, Northern Italy, AAPG Bulletin, v. 84, p.314-344.

Austin, N.J., Kennedy, L.A., Logan, J.M., and Rodway, R., 2005, Textural controls on the brittle deformation of dolomite; the transition from brittle faulting to cataclastic flow, Geological Society, London, Special Publications, v. 243, p. 51-66.

Bazalgette, L., 2004, Relations plissement/fracturation multi-échelle dans les multicouches sédimentaires du domaine élastique/fragile: accommodation discontinue de la courbure par la fracturation de petite échelle et par les articulations. Possibles implications dynamiques dans les écoulements des reservoirs [Dissertation], Montpellier, France, Université Montpellier II, 252 p.

Baud, P., Schubnel, A., and Wong, T.F., 2000, Dilatancy, compaction, and failure mode in Solnhofen limestone, Journal of Geophysical Research, v.105, p. 19,289-19,303.

Cleven, N., 2008, The Role of Dolomite Content on the Mechanical Strength and Failure Mechanisms in Dolomite-Limestone Composites [Dissertation], Vancouver, BC, University of British Columbia, 70 p.

Cooke, M.L., Simo, J.A., Underwood, C.A., and Rijken, P., 2006, Mechanical stratigraphic controls on fracture patterns within carbonates and implications for groundwater flow, Sedimentary Geology, v. 184, p. 225-239.

Cooke, M.L., and Underwood, C.A., 2001, Fracture termination and step-over at bedding interfaces due to frictional slip and interface opening, Journal of Structural Geology, v. 23, p. 223-238.

Di Naccio, D., Boncio, P., Cirilli, S., Casaglia, F., Morettini, E., Lavecchia, G., Brozzetti, F., 2004, Role of mechanical stratigraphy on fracture development in carbonate reservoirs: Insights from outcropping shallow water carbonates in the Umbria-Marche Apennines, Italy, Journal of Volcanology and Geothermal Research, v. 148, p. 98-115.

Eggenkamp, I., 2006, Jumping Pound West 1 Mississippian petrophysical update, Shell Internal Document [Unpublished manuscript], unknown p.

Eggenkamp, I., 2007, Jumping Pound West volumetric review, Shell Internal Document [Unpublished manuscript], unknown p.

Fermor, P., 1999, Aspects of the Three Dimensional Structure of the Alberta Foothills and Front Ranges, Geological Society of America Bulletin, v.111, p. 317-346.

Fredrich, J., Evans, B., and Wong, T.F., 1990, Effect of Grain Size on Brittle and Semibrittle Strength: Implications for Micromechanical modeling of Failure in Compression, Journal of Geophysical Research, v.95 p. 10,907-10,920.

Gaswirth, S.B., Budd, D.A., Crawford, B.A., 2006, Textural and stratigraphic controls on fractured dolomite in a carbonate aquifer system, Ocala limestone, west-central Florida, Sedimentary Geology, v. 184, p. 241-254.

Glass, D.J., Ed., 1997, Lexicon of Canadian Stratigraphy Volume 4 Western Canada, Including Eastern British Columbia, Alberta, Saskatchewan and Southern Manitoba. Calgary, AB: Canadian Society of Petroleum Geologists, 1423 p.

Martindale, W., and Boreen, T.D., 1995, Temperature stratified Mississippian carbonates as hydrocarbon reservoirs- examples from the Foothills of the Canadian Rockies, Proceedings of the Cool and Cold Water Carbonate Conference, Geelong, Australia, Geological Society of Australia, 20 p.

Michol, K.A., Russell, J.K., and Andrews, G.D.M., 2008, Welded block and ash flow deposits from Mount Meager, British Columbia, Canada, Journal of Volcanology and Geothermal Research v.169, p. 121-144.

Miller, D., Stephenson, B., Willet, A., Fraser, R., and Denike. C., 2007, Carbonate exploration in the Canadian Thrust Belt; fracture zone delineation in the Waterton area, EP Journal of Technology, Special Issue, v.09, p.19-24.

Nelson, C.S., ed., 1988, Non tropical shelf carbonates-modern and ancient: Sedimentary Geology, v.60, p51-70.

Ollerenshaw, N., 1978, Geology, Calgary, West of Fifth Meridian, Alberta-British Columbia, Geological Survey of Canada, "A" Series Map, 1457A, Scale: 1:125,000.

Palchik, V., and Hatzor, Y.H., 2000, Crack damage stress as a composite function of porosity and elastic matrix stiffness in dolomites and limestones, Engineering Geology, v. 63, p. 233-245.

Ruelle, J., 2008, Geological overview of the Mississippian Turner Valley, Shell Internal Document [Unpublished manuscript], 30 p.

Stephenson, B., Koopman, A., Hillgartner, H., McQuillan, H., Bourne, S., Noad, J., and Rawnsley, K., 2007, Structural and stratigraphic controls on fold-related

fracturing in the Zagros Mountains, Iran: Implications for reservoir development, Geological Society, London, Special Publications, v. 270, p. 1-21.

Van der Pluijm, B.A., and Marshak, S., 2003, Earth Structure: An Introduction to Structural Geology and Tectonics, New York, W W Norton, 674 p.

Wittstock, M, 2008, Characterization of natural fracture permeability in the Jumping Pound West (JPW1 & JPW2) Field, Shell Internal Document [Unpublished manuscript], 42 p.

Whole rock geochemistry, ALS Chemex: http://www.alsglobal.com/Mineral/ALSContent.aspx?key=53 (27 February 2009).

8. 0 APPENDIX A: TABLES

Table 6: Bulk Composition

Sample Number	Total Mass (kg)	SiO_2 %	Al_2O_3 %	Fe_2O_3 %	CaO %	MgO %	Na_2O %	K_2O %	Cr_2O_3 %	TiO_2 %	MnO %	P_2O_5 %	SrO %	BaO %	LOI %	Total
Mt1-B-40%	0.24	6.24	1.10	0.47	32.03	15.67	0.12	0.35	<0.01	0.03	<0.01	0.034	0.01	<0.01	42.2	98.26
Mt2-9-28%	0.18	30.77	1.77	0.28	19.58	14.03	0.13	1.00	<0.01	0.11	0.01	0.033	0.01	0.01	30.9	98.62
Mt3-14-50%	0.20	9.58	1.85	0.34	26.54	18.14	0.13	0.59	0.01	0.06	<0.01	0.02	0.01	<0.01	41.0	98.27